https://doi.org/10.5194/essd-2026-513
Preprint. Discussion started: 9 September 2026

Open Access Earth System Science Data Discussions

3D crustal model of Southern Apennines (Italy) by integrating geological, geophysical and petrophysical constraints

Maddalena Perrini[1], Grazia De Landro[2,*], Gianluca Gola[3], Filippo Accomando[4], Maurizio Fedi[5], Vanja Kastelic[6], Pietro Tizzani[7], Deborah Di Naccio[6], Michele M.C. Carafa[6], Giuseppe Falcone[8], Matteo Taroni[8], Aldo Zollo[2] and Raffaele Castaldo[4]

[1]*Dipartimento di Scienze della Terra, Università degli Studi di Torino, Turin, Italy (maddalena.perrini@unito.it)*
[2] *Dipartimento di Fisica "Ettore Pancini", Università degli Studi di Napoli, "Federico II", Naples, Italy*
[3] *Istituto di Geoscienze e Georisorse (IGG), CNR, Turin, Italy*
[4] *Istituto per i Sistemi Agricoli e Forestali del Mediterraneo (ISAFoM), CNR, Portici, Italy*
[5] *Dipartimento di Scienze della Terra (DiSTAR), Università degli Studi di Napoli "Federico II", Naples, Italy*
[6] *Istituto Nazionale di Geofisica e Vulcanologia (INGV), L'Aquila, Italy*
[7] *Istituto per il Rilevamento Elettromagnetico dell'Ambiente (IREA), CNR, Naples, Italy*
[8] *Istituto Nazionale di Geofisica e Vulcanologia (INGV), Roma, Italia*

Correspondence to: Grazia De Landro (grazia.delandro@unina.it)

Abstract. The Southern Apennines in Italy represent a geologically complex and seismically active region shaped by the ongoing convergence between the African and Eurasian plates. In this study, we present a high-resolution 3D crustal model of the Southern Apennines, parameterized on a 5 × 5 × 1 km³ grid and constructed through the systematic integration of geological, geophysical, and petrophysical data. The considered dataset includes laboratory velocity measurements (v_p) under different pressure and temperature conditions, stratigraphic well logs, seismic tomography (v_p), and geophysical models from inversion of gravimetric and magnetic data. Pressure- and temperature-dependent corrections were applied to P-wave velocities derived from regional seismic tomography, enabling us to delineate key intra-crustal boundaries, including the top of the Mesozoic limestones, the base of the Mesozoic sedimentary succession, the onset of the felsic crystalline basement, and the deeper transition to mafic, gabbroic lower-crustal units, within a 3D volume extending down to the Moho discontinuity. This modelling strategy ensures full internal consistency across spatial scales and tectonic domains, and is validated using independent borehole data, receiver functions, and other geophysical interpretations. The resulting 3D volume offers a robust framework for investigating crustal architecture and supports applications in geophysical modeling and seismic hazard assessments. All datasets are openly accessible under FAIR principles, promoting transparency, reproducibility, and interdisciplinary reuse of the results.

https://doi.org/10.5194/essd-2026-513
Preprint. Discussion started: 9 September 2026

Open Access Earth System Science Data Discussions

1. Introduction

Accurate reference models of the crust have been useful for potential field modeling (Yegorova & Starostenko, 2002), forward simulations of seismic wave propagation (e.g., Capdeville & Marigo, 2008; Masson and Virieux, 2023), and the precise location of seismic events (e.g.,Muzellec et al. 2025; De Landro et al. 2025), but they also play a crucial role in advanced numerical simulations for ground motion evaluation, seismic hazard assessment, resource exploration, and heat flow studies. Such broad applications increasingly demand 3D reference models that can capture the structural complexity and heterogeneity of the crust across multiple spatial scales. The construction of this kind of model needs the integration of complementary datasets (Goleby et al. 2006; Molinari et al. 2011, Granado et al. 2021; Camanni et al. 2025), and this interdisciplinary synthesis represents a critical step to account for the heterogeneity of the crust and for ensuring a geologically consistent representation of the subsurface.

The Southern Apennines is one of the most seismically active and geologically complex regions in Italy, making it a critical natural laboratory for seismic hazard assessment, geodynamic research, and the construction of integrated geophysical and geological models. The Southern Apennines form a complex orogenic system shaped by lithospheric convergence, crustal delamination, and post-collisional processes, including lithospheric thinning, magmatism, and mantle upwelling. The region's heterogeneous crust comprises distinct geological domains with marked differences in stratigraphic architecture and mechanical properties, whose spatial arrangement controls deformation styles, thrust geometries, and crustal stacking (Cello and Mazzoli, 1998; Mazzoli et al., 2000; Menardi Noguera and Rea, 2000; Improta et al., 2000; Catalano et al., 2004; Nicolai and Gambini, 2007). This area is further characterized by active fault systems, high geothermal gradients, and significant hydrocarbon reservoirs, making it a natural laboratory for both fundamental and applied geoscience.

Despite the availability of extensive geological and geophysical datasets for the Southern Apennines, including ViDEPI exploratory wells from the Italian project "*Visibilità dei Dati afferenti all'attività di Esplorazione Petrolifera in Italia*", seismic reflection profiles (Mostardini and Merlini, 1986; Scrocca et al., 2007), tomographic models (Di Stefano and Ciaccio, 2014; Magnoni et al., 2022), and potential field data (Kelemework et al., 2021a), as well as a comprehensive literature on the structural framework at both regional and local scales, an integrated 3D crustal model of the Southern Apennines is still lacking, largely because such models are particularly challenging to construct in this structurally complex region. Existing studies are typically restricted to local domains or specific geological targets (e.g., Feriozzi et al., 2024), preventing the development of a regionally consistent crustal framework. This limitation currently constrains comparative and large-scale geophysical analyses across the Southern Apennines orogenic system.

In this study, we present an integrated 3D crustal model beneath the Southern Apennines, built on a regular (5 × 5 × 1) km³ grid, combining geological data, geophysical models and petrophysical constraints to reconstruct the internal crustal structure. The integrated model is designed to capture the regional-scale structural framework, rather than resolving local geometric complexity, ensuring geological consistency, and its reproducibility. To constrain intra-crustal discontinuities, we combine seismic tomography (Magnoni et al., 2022), which, unlike 1D well logs and 2D seismic sections or geophysical surfaces, provides the only fully 3D and spatially continuous coverage for the entire study area, with laboratory P-wave velocity measurements across representative lithologies. The analysis presented here is based primarily on the P-wave velocity model of Magnoni et al. (2022). While corresponding Vs and Vp/Vs models are available, their spatial resolution is less homogeneous and their interpretation may be more strongly influenced by secondary effects such as fluids, attenuation, and anisotropy,

https://doi.org/10.5194/essd-2026-513
Preprint. Discussion started: 9 September 2026

Open Access Earth System Science Data Discussions

making them less suitable for defining regional crustal discontinuities. The crustal model, extending from the topographic surface down to the Moho, incorporates the variable-thickness Mesozoic to Cenozoic sedimentary fill of the foredeep, the adjacent Mesozoic carbonate platforms, and their underlying Permo-Triassic crystalline basement. For delineation of the Moho geometry, we used the model proposed by Spada et al. (2013), constrained by using multiple sources, such as receiver function analyses (Piana Agostinetti and Amato, 2009; Savastano and Piana Agostinetti, 2019), iso-velocity surfaces extracted from tomography, and gravity models (Kelemework et al., 2021a). The tectonic evolution of the Calabrian Arc, characterized by Alpine-style nappe emplacement of African lithosphere, distinguishes it from the Apennines. Consequently, the Calabrian Arc is included in the spatial extent of the model, but its internal crustal structure is not fully detailed.

The validity and robustness of the retrieved 3D crustal model have been assessed through a systematic comparison with multiple independent datasets, including 2D seismic profiles, potential field surfaces, and well logs of stratigraphic information. This multi-dimensional, multi-parametric, and multidisciplinary validation framework ensures that the model is consistent with the full range of geological and geophysical constraints available for the study area.

The block-based workflow in Fig. 1 summarizes the main phases of the modeling process, leading to a validated crustal model of the Southern Apennines that ensures reproducibility and supports its application in comparable geodynamic environments.

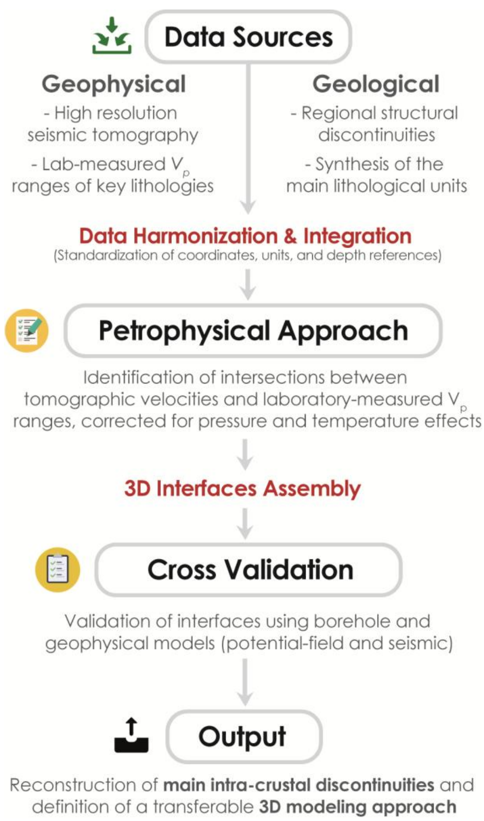

https://doi.org/10.5194/essd-2026-513
Preprint. Discussion started: 9 September 2026

Figure 1: Workflow for constructing the 3D crustal model of Southern Apennines, Italy. Integrated geological data and geophysical models are processed following petrophysical constraints to delineate intra-crustal discontinuities and validated against borehole, potential-field, and seismic data, providing a transferable 3D modeling framework.

The paper is structured as follows. After introducing the regional geological and geodynamic framework of the study area, with emphasis on the main lithostratigraphic units and tectonic domains, we describe the multidisciplinary datasets and methodological workflow adopted for the construction of the 3D crustal model. This is followed by a detailed presentation of the model-building procedure and the validation strategy used to assess its geological and geophysical consistency. The results section presents the retrieved 3D crustal model and its validation against independent geological and geophysical observations. Finally, a comprehensive inventory of all datasets released with this study is provided in the Data Availability section, with detailed file-level documentation reported in Supplementary Notes SN1-SN6.

2. Geological setting

The Southern Apennines form a key segment of the central Mediterranean orogenic system, developed in response to the convergence between the African and European plates from the Late Cretaceous to the Quaternary (Boccaletti et al., 1990; Catalano et al., 2004). The evolution of the belt involved the progressive deformation of the Adria continental margin and associated basinal domains through subduction, nappe stacking, and subsequent extensional processes (Ghisetti and Vezzani, 1999; Carmignani et al., 2001; Vitale and Ciarcia, 2013) (Fig. 2).
The present-day crustal architecture consists of a stack of tectono-stratigraphic units, including (i) allochthonous accretionary complexes (Liguride and Sicilide units; e.g., Prosser et al., 2021), (ii) platform and basinal successions derived from the western Adria margin (e.g., Bosellini, 2004), and (iii) the Apulian carbonate platform forming the foreland domain (Ogniben, 1985; Cello and Mazzoli, 1998; Vezzani et al., 2010). These domains are organized above major thrust surfaces that define the large-scale structural framework of the belt (Mostardini and Merlini, 1986; D'Andrea et al., 1993; Monaco et al., 1998) (Fig. 2).
From a lithological perspective, the Apulian carbonate platform consists of a ~5-6 km thick succession of Mesozoic-Tertiary shallow-water carbonates (Ricchetti et al., 1980-1988; Cotecchia, 2014), overlying Permo-Triassic siliciclastic deposits (Verrucano Formation sensu Cassinis et al., 2007-2012 and Aldinucci et al., 2008), which in turn rest on the Hercynian crystalline basement (Menardi Noguera and Rea, 2000; Patacca and Scandone, 2007). The basal portion of the carbonate sequence includes Triassic evaporitic deposits (Burano Formation), characterized by dolomites and anhydrite levels, which provide a key stratigraphic marker within the model.
The Apenninic (Campano-Lucano) platform includes up to ~5 km of Late Triassic to Miocene shallow-marine carbonates, structurally involved in thrust sheets emplaced toward the foreland (Patacca et al., 2001). Basinal units (Lagonegro-Sannio-Molise domain) consist of deep-water sedimentary successions originally located between the Apenninic and Apulian carbonate platforms (Scandone, 1972; Carbone et al., 1988). These successions include radiolarites, micritic limestones, and siliceous formations, representing deep-marine depositional environments that contrast with the adjacent carbonate platforms. Liguride-Sicilide units include ocean-derived and basinal deposits associated with accretionary processes (Mostardini and Merlini, 1986; Casero et al., 1988; Knott, 1987).
A tectonic mélange layer, composed of deformed Miocene-Lower Pliocene sediments, is locally interposed between the Apenninic and Apulian domains and may reach thicknesses of several hundred meters to >1 km (Butler et al., 2004; Shiner et al., 2004; Ferranti et al., 2024; Feriozzi et al., 2024). The mélange includes blocks

derived from both basinal and platform units and is constrained by borehole and seismic data as a laterally continuous unit within the model domain.

Quaternary deposits and volcaniclastic sequences locally overlie the older units, particularly within extensional basins such as the Campania Plain, where sediment thickness may exceed 1 km (Cotecchia, 2014; Brozzetti et al., 2011).

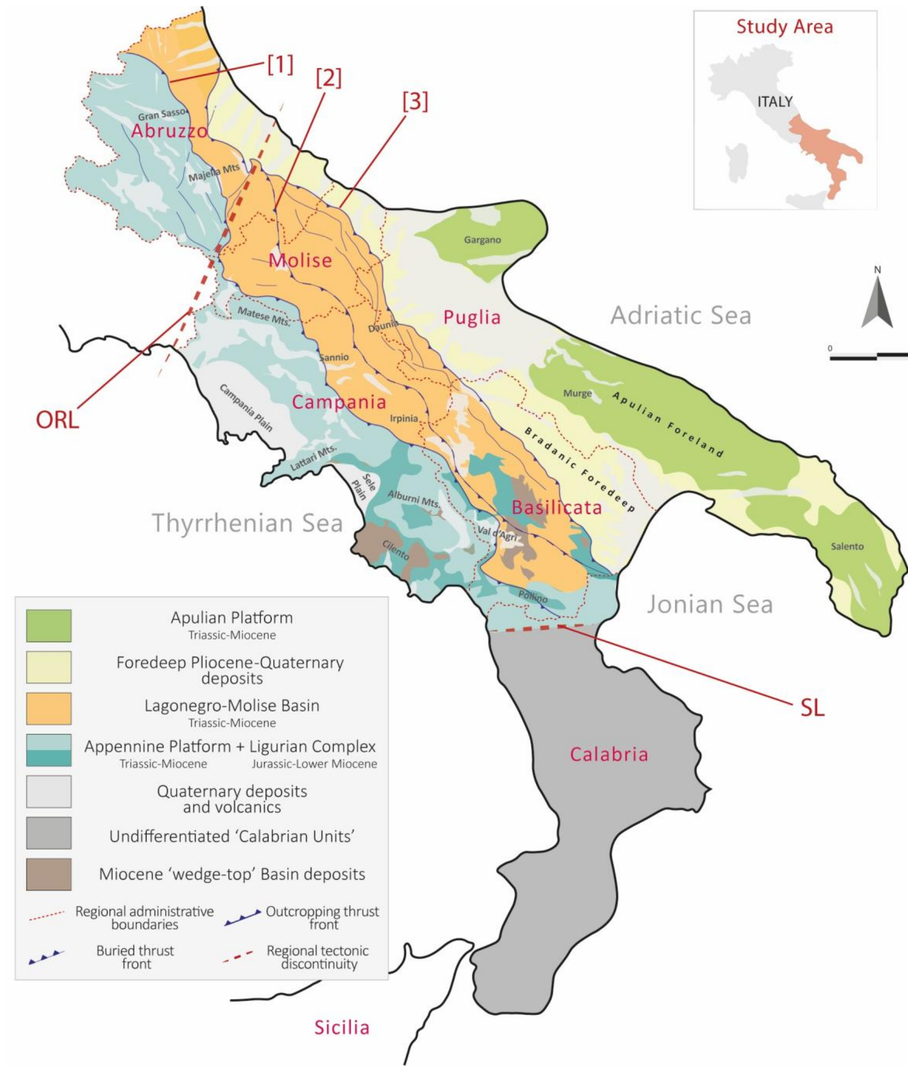

Figure 2: Conceptual geological framework. Simplified geological-structural setting used to define the principal intra-crustal discontinuities considered in this study. Domains were accreted above three principal thrust surfaces, with [1] and [3] outcropping and [2] buried (Vezzani et al., 2010). Key structures include the Ortona-Roccamonfina (ORL) and Sangineto (SL) tectonic lines. Adapted from Mostardini & Merlini (1986). The inset shows the location of the investigated Southern Apennines sector, Italy.

https://doi.org/10.5194/essd-2026-513
Preprint. Discussion started: 9 September 2026

Open Access Earth System Science Data Discussions

For the purpose of the 3D crustal modeling, the geological framework is simplified to retain only the lithological units that can be consistently resolved at regional scale and integrated with the available geophysical datasets. This simplification is guided by (i) the spatial resolution of the tomographic model, (ii) the need to preserve first-order lithological contrasts, and (iii) the heterogeneous distribution of geological constraints across the study area. Accordingly, the model includes the following main units (Fig. 3):

- Sedimentary cover, including Lagonegro-Sannio-Molise successions and Neogene-Quaternary deposits
- Mesozoic carbonate platform units, representing both the Apulian and Apenninic domains
- Permo-Triassic siliciclastic successions (Verrucano Formation), underlying the carbonate sequence
- Hercynian crystalline basement
- Lower crustal unit, extending down to the Moho discontinuity

This resulting reference simplified stratification (Fig. 3b,c). preserves the main lithological contrasts relevant for regional-scale crustal modeling and is consistent with the resolution of the tomographic dataset, while providing the reference framework for defining intra-crustal discontinuities in the 3D model.

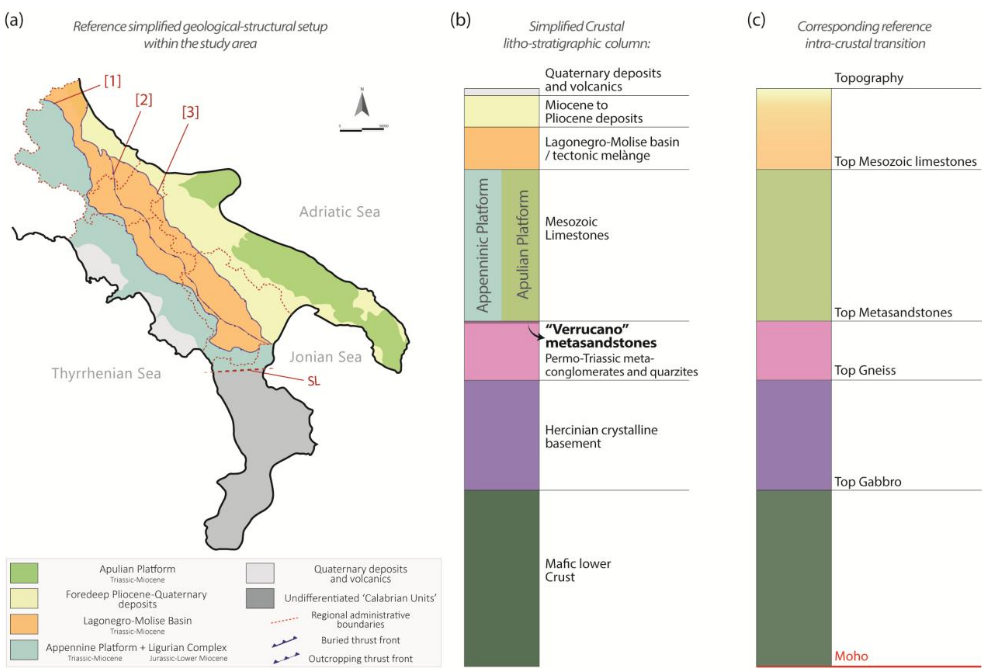

Figure 3: Synthesis of the main representative litho-stratigraphic units. (a) Simplified geological-structural setting of the Southern Apennines showing the main tectono-stratigraphic domains and the regional structural features (available in *Supplementary Note 4* of the Supplementary Material). The red dotted Sangineto Line (SL) is also shown as a major regional tectonic discontinuity. (b) Simplified litho-stratigraphic column representing the generalized crustal architecture beneath the Southern Apennines, synthesized from geological maps, borehole information, and previous regional studies. (c) Correspondence between the generalized litho-stratigraphic succession and the reference intra-crustal discontinuities used for the geological interpretation and construction of the three-dimensional crustal model. These surfaces include the tops of the Mesozoic carbonate platform, metasedimentary succession, crystalline basement, mafic lower crust, and the Moho discontinuity.

https://doi.org/10.5194/essd-2026-513
Preprint. Discussion started: 9 September 2026

Open Access Earth System Science Data Discussions

3. Multidimensional Datasets

This section describes the datasets used for the construction and validation of the three-dimensional crustal model of the Southern Apennines. For each dataset, information on data origin, acquisition methodology, spatial resolution, spatial coverage, and associated uncertainties is provided. The datasets employed as model inputs and independent validation constraints are summarized in Table 1. The integration of multiple geological datasets and geophysical models allows the definition of a consistent 3D crustal framework, ensuring compatibility between observations at different spatial scales and depths.

Table 1: **Data and Models used to construct and validate the 3D crustal model**. Datasets used to construct and validate the 3D crustal model. Datasets are classified according to their spatial dimensionality: 3D (volumetric models), 2D (surfaces and sections), 1D (well data) and 0D (point measurements).

INPUT		
Dimensionality	**Dataset**	**Purpose**
3D	Seismic P-wave Tomographic Model (Magnoni et al., 2022)	To image crustal heterogeneities, recognize lithological discontinuities associated to elastic properties variations
2D	Digitized surface traces of major regional structures from Vezzani et al. (2010))	Used as geometric constraints for subsurface thrust reconstruction -
2D	Moho depth surface (Spada et al., 2013)	To define the crust-mantle boundary and provide 3D model lower geometric bound
2D	Topographic surface (Tarquini et al., 2023)	To define the upper 3D model geometric bound
0D	Laboratory v_p measurements	To define v_p ranges for representative crustal lithologies under specific pressure-temperature conditions

VALIDATION		
Dimensionality	**Dataset**	**Purpose**
2D	Gravity inversion model (Kelemework et al., 2021a)	To validate intra-crustal boundaries, crustal thickening, and lateral density variations
2D	Top Apulian Carbonate surface (Vezzani et al., 2010)	To validate depth of the top of carbonate sequences in the Apulian domain
2D	Top Campania-Lucania Carbonate platform (Kelemework et al., 2021a; Ferranti et al., 2024)	To validate the buried geometry of western (Appenninic) carbonate platform
2D	Interpreted seismic lines (CROP-04, CROP-11b,c)	To validate deep crustal structure, fault geometries, and thrust system architecture
1D	ViDEPI boreholes	To constrain lithostratigraphy, carbonate thickness, and foredeep sediment distribution

3.1 Seismic P-wave tomography

Seismic velocity data were extracted from the full-waveform adjoint tomography model developed by Magnoni et al. (2022), which resolves the seismic structure of the crust and uppermost mantle across Southern Italy. The model

https://doi.org/10.5194/essd-2026-513
Preprint. Discussion started: 9 September 2026

Open Access Earth System Science Data Discussions

was generated through a high-resolution inversion of broadband seismic waveform data, sensitive to structure from the surface down to ~80 km depth, with optimal resolving power in the 5-45 km depth range. The inversion incorporated waveforms from 163 regional earthquakes (Mw 3.0-5.8), recorded at 412 permanent broadband stations between 2005 and 2014. The initial model was based on the 3D crustal velocity structure developed by Di Stefano and Ciaccio (2014). The adjoint method utilizes 3D sensitivity kernels and waveform misfits to iteratively update the velocity field, exploiting complete seismic waveforms, including later-arriving phases, rather than only first-arrival travel times.

In the original implementation, the model is discretized on an unstructured hexahedral mesh with a characteristic element size of ~5 km near the surface, increasing with depth, and is resolved at a minimum numerical period of approximately 10 s (Magnoni et al., 2022). In detail, the horizontal resolution in the investigated area varies between 5 and 20 km, depending on local raypath density and network geometry. The model achieves a vertical resolution of approximately 3-5 km in the upper crust (0-20 km) and around 5-7 km in the mid-crust down to the Moho (20-35 km). At depths exceeding ~45 km, resolution degrades rapidly due to limited ray coverage and increased parameter trade-offs (Fig. 4). The spatial resolution is therefore anisotropic and depth dependent.

For the purposes of this study, the tomography was first clipped using the study-area boundary extended by an approximately 10 km buffer (Fig. 4). This buffer was introduced to reduce boundary effects during the subsequent construction of the integrated 3D geological model. The resulting tomography domain was then resampled onto a regular 5 × 5 × 1 km grid extending down to 50 km depth, yielding 211,308 individual cells. The tomographic model was resampled onto a regular grid by aggregating the velocity values associated with the original model nodes within each cell of the target grid. A representative velocity value was assigned to each cell based on the statistical distribution of the original values, ensuring a consistent mapping onto the regular grid. This discretization was adopted to ensure consistency with the parametrization of the 3D model and to facilitate integration with independent geological and geophysical datasets. The choice of grid spacing considers the depth-dependent resolution of the seismic tomographic model and provides a homogeneous spatial framework for subsequent analysis. The resulting gridded velocity volume is subsequently used to extract P-wave velocity isosurfaces corresponding to major crustal interfaces and is provided as part of the derived datasets associated with this study. The original tomography model of Magnoni et al. (2022), together with the resampled version used in this study and the associated metadata describing the resampling procedure and model discretization, are available in *Supplementary Note 1* of the Supplementary Material.

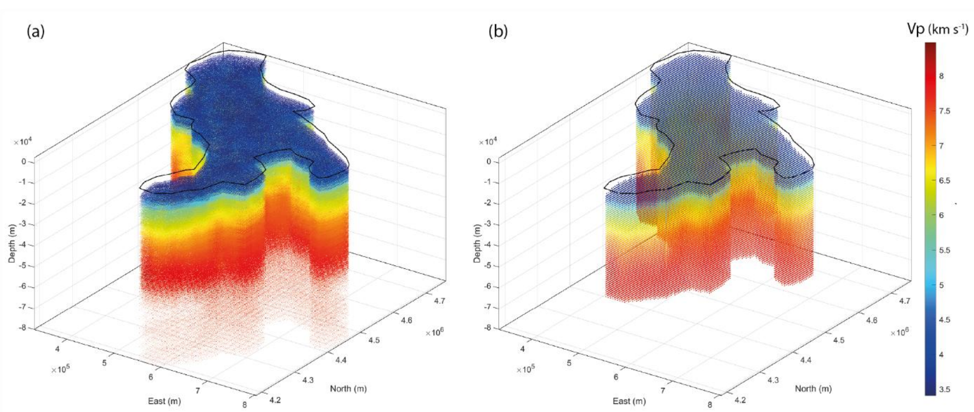

https://doi.org/10.5194/essd-2026-513
Preprint. Discussion started: 9 September 2026

Open Access Earth System Science Data Discussions

Figure 4. Seismic tomographic model horizontal discretization. Visual comparison between the original tomography dataset and the resampled tomography model used in this study. The black outline delineates the study area extended by a 10 km coastal buffer. (a) Original tomography nodes within the buffered study area. (b) Resampled tomography on a regular 5 km × 5 km × 1 km grid. The resampled model contains approximately 1/16 of the nodes of the original dataset (211,308 vs. 3,430,752 nodes), while preserving the original spatial extent, depth coverage, and overall three-dimensional geometry.

3.2 DEM of the study area

The upper boundary of the 3D model is defined by the topography of the Southern Apennines, derived from the TINITALY 1.1 digital elevation model (Tarquini et al., 2023). The DEM, provided at a spatial resolution of 10 m, was clipped to the study area (black buffer shown in Fig. 4) and used directly as the upper boundary of the integrated 3D geological model. Both the original TINITALY DEM and the clipped DEM adopted in this study are provided in *Supplementary Note 2* of the Supplementary Material.

3.3 Moho depth

The crust-mantle boundary (Moho) was defined using the near-3D Moho depth model proposed by Spada et al. (2013), which integrates controlled-source seismology (CSS) profiles and receiver function (RF) analyses across the Italian region. The dataset includes CSS constraints from national seismic experiments such as the CROP project (Scrocca et al., 2003) and regional surveys (Brueckl et al., 2010; Di Stefano et al., 2011; Waldhauser et al., 1998), combined with RF-derived Moho depth estimates from the Italian Seismic Network (Piana Agostinetti and Amato, 2009) and the Western Alps (Lombardi et al., 2008). A classification and weighting scheme was applied to the input data to account for variable data quality and associated uncertainties, following the methodology proposed by Waldhauser (1996) and Waldhauser et al. (1998). The authors interpolated the Moho surface on a regular grid with a horizontal spacing of 6 × 6 km² and a vertical sampling of 2 km, using a minimum roughness criterion. Reported uncertainties range from ±3 km in well-constrained areas to ±10 km in regions with sparse data coverage or complex crustal structure.

In this study, the Moho surface was resampled onto the 5 × 5 km grid adopted for the 3D model (Fig. 2), ensuring consistency with the overall geometric parametrization. The original RF constraints of Spada et al. (2013) were also preserved in tabular form, including preferred and alternative Moho estimates (Mo1 and Mo2), intracrustal discontinuities (InCr), and the associated ±1σ uncertainty bounds. These station-based measurements provide independent constraints for model validation and are complemented by P-wave velocities extracted from the tomography of Magnoni et al. (2022), allowing direct comparison between RF-derived discontinuity depths and tomography-derived seismic velocities.

In addition to the original Moho surfaces of Spada et al. (2013), *Supplementary Note 3* of the Supplementary Material includes the description of the complete station-by-station comparison between RF-derived Moho depths and P-wave velocities extracted from the tomography of Magnoni et al. (2022), together with all associated downloadable files and metadata.

3.4 Relevant structural features

Regional structural features were derived from the geological framework proposed by Vezzani et al. (2010), which provides a synthesis of the main tectonic discontinuities in the central-southern Apennines (Fig. 2). In particular, the traces of the main thrust fronts were extracted from the regional geological map, including: (i) the thrust front of the Lazio-Abruzzi and Campania-Lucania carbonate platforms (labeled [1] in Fig. 2), (ii) the buried thrust front

https://doi.org/10.5194/essd-2026-513
Preprint. Discussion started: 9 September 2026

of the Apulia-Adriatic domain (labeled [2]), and (iii) the external thrust front of the Apenninic fold-and-thrust belt (labeled [3]).

These structural features define major boundaries between tectono-stratigraphic domains characterized by distinct geological and geophysical properties. Their surface traces were used as reference constraints to guide the lateral subdivision of the model domain.

The geometry of these discontinuities at depth was approximated based on published regional cross-sections and structural models (e.g., Bonardi et al., 1988; Cosentino et al., 2003; Patacca and Scandone, 2007; Mazzoli et al., 2008), ensuring consistency between surface geology and subsurface representation.

In the southern sector, the Sangineto Line (Ghisetti and Vezzani, 1981) was also considered as a major structural boundary separating the Apenninic domain from the Calabrian Units (Amodio Morelli et al., 1976).

These structural elements were incorporated into the 3D model as geometrical constraints to define the spatial organization of the main crustal units and to ensure coherence with the regional tectonic framework.

The adopted structural framework is defined at regional scale and reflects the level of detail of the source geological maps and cross-sections. As such, these features are used as first-order geometrical constraints rather than high-resolution representations of individual fault geometries. The digitized surface traces of major regional structures in Fig.3 (labeled as [1], [2] and [3] are available in *Supplementary Note 4* of the Supplementary Material).

3.5 Laboratory measurements of seismic P-wave velocity on relevant lithologies

Experimental P-wave velocity (vp) data were compiled from published laboratory studies on representative crustal lithologies (Fountain, 1976; Kern and Richter, 1981; Kern and Schenk, 1985; Burke and Fountain, 1990; Wepfer and Christensen, 1991; Kern et al., 1996; Khazanehdari et al., 2000; Barberini et al., 2007; Kono et al., 2009; Wang et al., 2013). The dataset includes measurements performed under controlled pressure and temperature conditions, allowing characterization of vp as a function of physical parameters (Fig. 5).

The compiled data consist of directional P-wave velocity measurements along three orthogonal axes of cubic samples, together with density and mineralogical information. The dataset spans a wide range of lithologies, including sedimentary, metamorphic, and igneous rocks representative of upper crust, lower crust, and upper mantle domains. Most samples derive from exposed crustal sections of the Ivrea-Verbano and Strona-Ceneri Zones (Southern Alps), southern Calabria, and additional reference areas including the North China Craton and Scandinavian Lapland. Measurements were performed using pulse-transmission techniques (1-2 MHz) under confining pressures up to 600-1000 MPa and, in selected cases, at elevated temperatures under high confining pressure conditions.

From the compiled datasets, the linear segments of the vp-pressure and vp-temperature relationships were extracted using published best-fit regressions, characterized by high coefficients of determination (average $R^2 \approx 0.96$). The resulting dataset includes vp at ambient conditions (vp_0), pressure derivatives ($\partial vp/\partial P$), and temperature derivatives ($\partial vp/\partial T$).

The final dataset comprises 175 pressure derivatives and 119 temperature derivatives. A statistical summary of these values is reported in Table 2, including mean values and standard deviations for each lithology. Based on these data, and in accordance with the simplified lithostratigraphic column (Fig. 3c), we selected only the lithologies shown in bold as representative end-members for our modeling: limestone for the carbonate platform domain, sandstone for the slightly metamorphosed siliciclastic successions of the Verrucano Formation, felsic

https://doi.org/10.5194/essd-2026-513
Preprint. Discussion started: 9 September 2026

Open Access Earth System Science Data Discussions

gneiss for the felsic crystalline upper crust, gabbro for the mafic lower crust, and peridotite for the ultramafic upper mantle. These velocity values are used to ensure consistency between laboratory-derived physical properties and the velocity ranges associated with the modelled crustal units. The original and processed datasets supporting the petrophysical analysis, including the files used to derive the velocity intervals reported in Table 2 and to reproduce the pressure- and temperature-correction curves shown in Fig. 5, are fully documented and made available in *Supplementary Note 5* of the Supplementary Material.

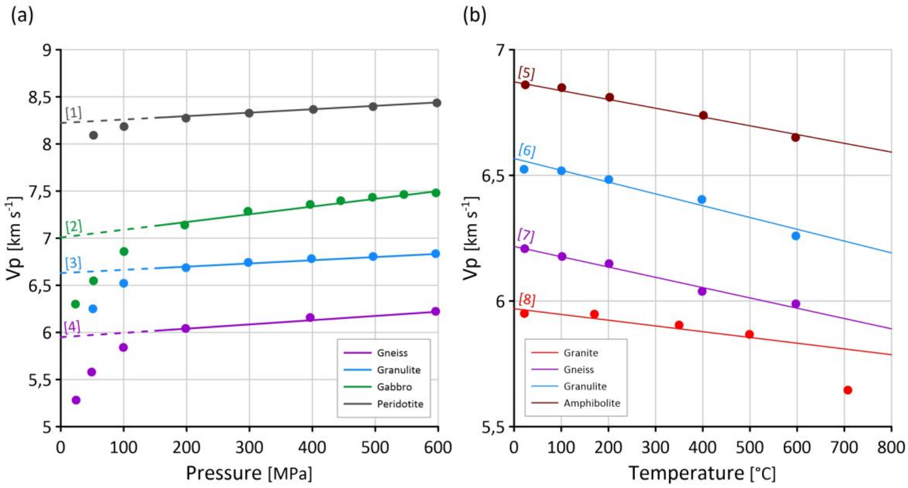

pressure-dependent correction

ID	Rock type	Reference
[1]	Peridotite	*Burke & Fountain (1990)*
[2]	Gabbro	*Wang et al. (2013)*
[3]	Granulite	*Burke & Fountain (1990)*
[4]	Gneiss	*Kern et al. (1996)*

temperature-dependent correction

ID	Rock type	Reference
[5]	Amphibolite	*Kern et al. (1996)*
[6]	Granulite	*Kern et al. (1996)*
[7]	Gneiss	*Kern et al. (1996)*
[8]	Granite	*Kern & Richter (1981)*

Figure 5: Dependence of P-wave velocity on pressure and temperature in representative rock types. (a) Experimental compressional wave velocity data as a function of pressure and (b) temperature for representative rock samples. (c) Summary table listing the lithotypes, data sources, and coefficients of the best-fit linear regressions reported in panels (a) and (b).

Table 2: Statistics of pressure and temperature derivatives of P-wave velocities of various lithologies representative of upper crustal (UC), lower crustal (LC) and upper mantle (UM) layers. The average values of density (ρ in [kg m^{-3}]), P-wave velocity of the nonporous rock at ambient conditions (v_{p0} in [km s^{-1}]), the pressure ($\partial v_p/\partial P$ in [1×10^{-4} km s^{-1} MPa^{-1}]) and temperature ($\partial v_p/\partial T$ in [1×10^{-4} km s^{-1} °C^{-1}]) derivative are reported together with the 1-sigma (in brackets). As detailed in the section 2 and Fig. 3c, we reported in bold the lithologies selected as representative of the lithostratigraphic units used in the crustal-scale synthesis.

Location	Rock	Classification	Composition	ρ	v_{p0}	$\partial v_p/\partial P$	$-\partial v_p/\partial T$
UC	Granite	Intrusive	Felsic	2666 (62)	6.07 (0.26)	5.78 (2.71)	2.49 (0.40)
UC	**Gneiss**	**Metamorphic**	**Felsic**	**2859 (154)**	**6.28 (0.34)**	**3.57 (0.97)**	**3.55 (1.11)**
UC	Gneiss	Metamorphic	Silicoclastic	2802 (194)	6.20 (0.48)	5.08 (3.05)	5.18 (0.89)
UC	Schist	Metamorphic	Silicoclastic	2760 (43)	5.19 (1.61)	4.33 (3.81)	5.30 (2.00)

https://doi.org/10.5194/essd-2026-513
Preprint. Discussion started: 9 September 2026

UC	**Meta-sandstone**	**Sedimentary**	**Silicoclastic**	**2580 (20)**	**5.32 (0.76)**	**6.88 (3.21)**	**2.54 (0.01)**
UC	**Limestone**	**Sedimentary**	**Carbonate**	**2725 (10)**	**5.05 (1.74)**	**1.19 (0.67)**	**6.37 (0.01)**
LC	**Gabbro**	**Intrusive**	**Mafic**	**2982 (130)**	**6.88 (0.20)**	**3.37 (1.12)**	**2.88 (1.51)**
LC	Amphibolite	Metamorphic	Mafic	2990 (96)	6.74 (0.22)	5.21 (2.94)	2.65 (0.97)
LC	Granulite	Metamorphic	Felsic	2823 (4)	6.40 (0.09)	3.15 (0.88)	2.66 (0.18)
LC	Granulite	Metamorphic	Mafic	3047 (147)	6.79 (0.38)	2.91 (1.47)	3.54 (1.40)
LC	Granulite	Metamorphic	Silicoclastic	2932 (121)	6.62 (0.37)	3.64 (1.17)	5.07 (1.57)
UM	Pyroxenite	Intrusive	Ultramafic	3267 (47)	7.67 (0.38)	2.46 (1.25)	2.33 (0.90)
UM	**Peridotite**	**Intrusive**	**Ultramafic**	**3276 (29)**	**7.95 (0.31)**	**3.23 (0.87)**	**4.32 (1.14)**

3.6 Potential field data

The 3D gravity inversion model of Kelemework et al. (2021a) was used as an independent dataset to validate the geometry of major crustal interfaces derived from the 3D model. The model is based on Bouguer gravity anomalies compiled from both offshore and onshore measurements covering the Southern Apennines and adjacent regions. The original dataset was homogenized using a reference density of 2.6 g/cm³, and terrain corrections were applied using a 100 m-resolution digital elevation model (DEM). The grid spacing of the gravity dataset is 1 km. The inversion was performed using nonlinear 3D techniques (Fedi, 1997), which allow the reconstruction of subsurface density interfaces from potential field data. The inversion was constrained using independent datasets, including seismic models and borehole information, applied over subdivided regions of the study area.

For deeper crustal structures, spectral analysis of Bouguer anomalies was performed using a moving window approach, following the statistical model theory introduced by Spector and Grant (1970) and further developed by Fedi et al. (1997) and Kelemework et al. (2021b).

To enable quantitative validation within a common spatial framework, the gravity-derived surfaces were interpolated onto the (5 × 5 × 1) km³ grid adopted in this study. These surfaces were then compared with the corresponding interfaces derived from the 3D model. The gravity model is therefore used as an independent validation dataset to assess the consistency of the 3D model geometry. The corresponding potential-field-derived surfaces are documented in *Supplementary Note 6* of the Supplementary Material.

3.7 Controls on thickness of the Carbonatic Units

The thickness and geometry of the Mesozoic carbonate platforms underlying the Southern Apennines were constrained using a combination of geological, geophysical, and borehole datasets. These include regional geological maps (Fig. 2), borehole data from the ViDEPI database, and geophysical models derived from seismic tomography and gravity inversion (e.g., Kelemework et al., 2021b; Ferranti et al., 2024).

The Apulian carbonate platform is characterized by a regional westward deepening trend, with the top of the carbonate sequence ranging from less than 2 km in the foreland to more than 7 km beneath the thrust belt (Vezzani et al., 2010; Nicolai and Gambini, 2007). Borehole data from the ViDEPI database provide direct constraints on carbonate thickness and stratigraphy, particularly in the foreland domain. The base of the carbonate sequence is locally constrained by the occurrence of Permo-Triassic siliciclastic deposits (Verrucano Formation), which are used as a reference marker for the transition to the underlying basement (Fig. 3b and c).

https://doi.org/10.5194/essd-2026-513
Preprint. Discussion started: 9 September 2026

The Campania-Lucania carbonate platform exhibits a more complex geometry, with the top of the carbonate units generally located between 3 and 8 km depth, as constrained by integrated geophysical models (Kelemework et al., 2021a; Trumpy et al., 2022; Ferranti et al., 2024).
Seismic tomography provides additional constraints on the depth distribution of carbonate units through the identification of characteristic P-wave velocity ranges associated with carbonate lithologies (Amoroso et al., 2014; Feriozzi et al., 2024). In this study, velocity ranges between approximately 3.5 and 6.5 km/s were used as reference values to approximate the carbonate sequence within the 5 x 5 x 1 km^3 reference seismic tomographic model.
The thickness and geometry of the carbonate units were defined by integrating these independent constraints within a common 3D framework (Fig. 3), ensuring consistency among geological observations, borehole information, and geophysical models. *Supplementary Note 6* of the Supplementary Material (Table 3) documents and provides the independent validation datasets used in this study, including borehole-derived depths and the interpolated surface defining the top of the Apulian carbonate platform (Vezzani et al., 2010), as well as the original point datasets and corresponding interpolated surfaces from Kelemenwork et al. (2021a) and Trumpy et al. (2022).

3.9 ViDEPI dataset

Lithostratigraphic constraints were derived from borehole data available in the ViDEPI database (https://www.videpi.com/videpi/videpi.asp), which provides access to subsurface information from hydrocarbon exploration activities in Italy. The dataset includes well logs, stratigraphic descriptions, and final reports from deep wells distributed across the Southern Apennines and adjacent regions.
In this study, a selection of deep wells was analyzed to extract key stratigraphic markers, with particular focus on the top and base of the Mesozoic carbonate units and on the distribution of foredeep and Neogene-Quaternary deposits. The identification of these markers was based on the lithostratigraphic descriptions provided in the original well documentation.
Particular attention was given to distinguishing carbonate units belonging to the Apulian Platform from those of the Campania-Lucania domain, where possible. The occurrence of Permo-Triassic siliciclastic deposits (Verrucano Formation) was used as a reference marker for the base of the carbonate sequence.
The extracted stratigraphic information was used to provide point-wise constraints on the depth and thickness of the main lithological units within the study area. These constraints were integrated within the 3D model framework to ensure consistency with borehole observations.
The subset of ViDEPI boreholes intersecting the Mesozoic carbonate platform is provided in *Supplementary Note 6* of the Supplementary Material (Table 3) as a tabulated dataset (Figs. 9-10), including well identifiers, UTM coordinates, cumulative distance along the selected profiles, and depths to the top of the carbonate units (m b.s.l.).

3.8 Interpreted seismic lines

Deep seismic reflection profiles from the CROP (CROsta Profonda) project (Finetti, 2005) were used as independent constraints on the geometry of crustal structures in the Southern Apennines. In particular, the CROP-04 and CROP-11b,c transects provide large-scale images of the crustal architecture across the orogenic belt and adjacent foreland domains. These profiles have been extensively interpreted in previous studies (e.g., Scrocca et al., 2003; Patacca and Scandone, 2001; Nicolai and Gambini, 2007; Mazzoli et al., 2013), and represent a key reference dataset for the geometry of major crustal interfaces and thrust systems.

https://doi.org/10.5194/essd-2026-513
Preprint. Discussion started: 9 September 2026

In this study, the interpreted seismic sections are used as qualitative constraints to assess the geometry and continuity of the main crustal boundaries within the 3D model. Their use is limited to first-order structural consistency, given the inherent variability among different interpretations and the absence of a unique subsurface model.

https://doi.org/10.5194/essd-2026-513
Preprint. Discussion started: 9 September 2026

4. Method

The 3D crustal model is constructed by considering a petrophysical relation between seismic v_p tomography and laboratory-derived P-wave velocity ranges for specific lithologies, which are the ones shown in the simplified lithostratigraphic framework in Fig. 3c. Each lithological unit is associated with characteristic P-wave velocity ranges derived from laboratory measurements (Table 2), representative of the main crustal domains, including carbonate units, siliciclastic successions, crystalline basement, and lower crustal lithologies.

The classification accounts for the dependence of seismic velocity on pressure and temperature conditions associated with crustal depths, allowing definition of in-situ velocity ranges for each lithological unit. The approach is first applied along 1D vertical profiles to identify depth intervals corresponding to the main lithological domains, and subsequently extended to the full 3D model grid. Each model cell is therefore assigned to a lithological unit based on its v_p value after applying these corrections. Key intra-crustal discontinuities are identified as surfaces separating adjacent lithological domains, corresponding to major contrasts between carbonate platforms, siliciclastic sequences, and crystalline basement units (Fig. 3c).

4.1 Pressure-Temperature corrections to seismic velocities

The compilation of laboratory-derived P-wave velocities representative of the main lithologies composing the considered crustal domains, including upper crust, lower crust, and lithospheric mantle (Fountain, 1976; Kern & Richter, 1981; Kern & Schenk, 1985; Burke & Fountain, 1990; Wepfer & Christensen, 1991; Kern et al., 1996; Khazanehdari et al., 2000; Barberini et al., 2007; Kono et al., 2009; Wang et al., 2013), together with their pressure and temperature derivatives, allowed the definition of in-situ velocity ranges for each lithological unit under crustal conditions. As discussed above, the lithologies selected as representative of the main crustal domains are highlighted in bold in Table 2, whereas the complete set of lithological correction curves is provided in *Supplementary Note 5*. Experimental data show that P-wave velocity increases with pressure and decreases with temperature, and that, for confining pressures exceeding ~150-200 MPa, both effects can be approximated as linear (Kern & Richter, 1981; Kern & Schenk, 1985). Under these conditions, the influence of microcrack closure is reduced, and the velocity response is dominated by the elastic properties of the rock matrix.

To account for these effects, pressure and temperature corrections were applied to the reference velocities using the following relationship:

$$v_p(z) = v_{p0}(z) + \frac{\partial v_p}{\partial p} \Delta p(z) + \frac{\partial v_p}{\partial T} \Delta T(z) \qquad (1),$$

where $v_p(z)$ is the in-situ compressional wave velocity at depth z, obtained by correcting the reference velocity $v_{p0}(z)$ for the effects of increasing pressure and temperature with depth. The first correction term $\Delta p(z)$ accounts for the increase in velocity due to lithostatic pressure scaled by the pressure derivative of v_p. The second correction term $\Delta T(z)$ reflects the decrease in velocity due to thermal effects, using the temperature increment (the local geotherm) and the thermal derivative of v_p. A thermal gradient was considered equal to 30 °C/km and to 22 °C/km for the western and eastern sector of the Southern Apennines, respectively (Della Vedova et al., 2001). Lithostatic pressure was computed assuming a layered crustal structure, with densities derived from seismic velocities (Ludwig et al., 1970; Brocher et al., 2005). Temperature was estimated using geothermal gradients of 30 °C/km and 22 °C/km for the western and eastern sectors of the Southern Apennines, respectively (Della Vedova et al., 2001).

https://doi.org/10.5194/essd-2026-513
Preprint. Discussion started: 9 September 2026

At shallow depths (< 5-6 km), corresponding to pressures below ~120-150 MPa, velocity variations are significantly influenced by porosity and compaction processes, particularly in sedimentary and carbonate units. In this depth range, the velocity-depth relationship was modeled using the Wyllie equation (Wyllie et al., 1956, 1958), which provides a valuable empirical tool to relate P-wave velocity (v_p) to porosity (θ) in fluid-saturated sedimentary rocks with relatively uniform mineralogy and under high effective pressure:

$$\frac{1}{v_p} = \frac{\theta}{v_{pw}} + \frac{1-\theta}{v_{p0}} \qquad (2),$$

where v_{pw} is the P-wave velocity in water, and v_{p0} is the P-wave velocity in the dry rock matrix. The resulting corrected velocity-depth relationships for the selected lithologies are shown in Fig. 6, where average values and ±1σ variability are reported for different thermal conditions. The grey-shaded area highlights the uppermost portion of the crust corresponding to the low-pressure domain, where porosity and compaction effects are accounted for through the Wyllie formulation.

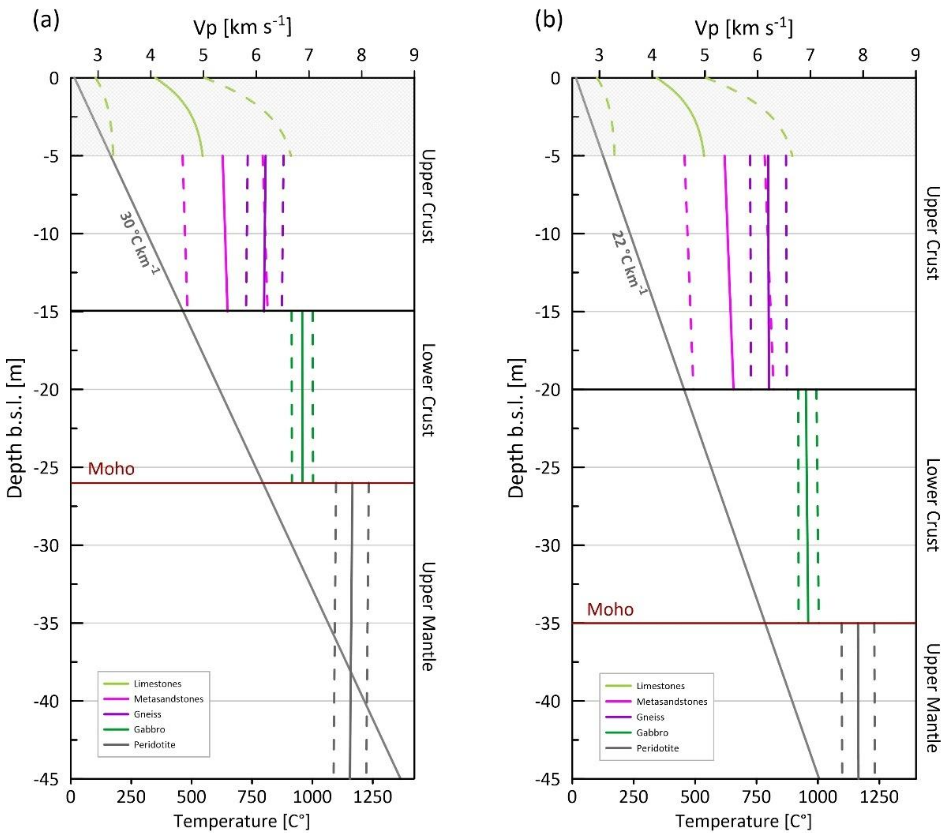

Figure 6: Velocity-depth profiles. The profiles are constructed using the dataset compiled through the literature review conducted in this work (see lithologies in bold in Table 2). The average (continuous line) and the ±1σ uncertainty (dashed lines) are displayed. The two thermal structures correspond to (a) a thinned crust (26 km) associated with a hot geotherm (grey line, geothermal gradient of 30 °C km^{-1}) and (b) a thick crust (35 km) associated with a cold geotherm (grey line, geothermal gradient of 22 °C km^{-1}).

https://doi.org/10.5194/essd-2026-513
Preprint. Discussion started: 9 September 2026

4.2 From 1D profiles to 3D crustal architecture

The proposed petrophysical relation between seismic vp tomography and laboratory-derived P-wave velocity ranges used to classified the specific lithologies, here defined petrophysical approach, was initially applied along vertical 1D profiles to identify depth intervals corresponding to the main lithological units, based on the intersection between tomographic velocities and the reference velocity ranges defined for each lithology (Fig. 6; Table 2). This procedure allows the identification of key transitions within the crust, including the top of carbonate units, the transition to siliciclastic successions (e.g., Verrucano-type deposits), and the onset of crystalline basement units. An example of this approach is shown in Fig. 7, where a vp profile extracted from the tomographic model is compared with the velocity ranges of representative lithologies (Table 2), together with borehole data from the Acerno 1 well (ViDEPI dataset; Ferranti et al., 2024). The comparison illustrates how intersections between tomographic velocities and reference lithological ranges can be used to define depth intervals associated with major lithological units in the shallow crust, providing a consistency check with independent borehole information.

In this framework, the reference velocity values used for classification correspond to the central v_{p0}values for each lithology, while the minimum and maximum bounds are used to define the variability range associated with each unit (Table 2; Fig. 6). This approach allows accounting for the intrinsic variability of lithological properties, particularly for carbonate units, which are characterized by a wide range of seismic velocities. The intersection between the lithology-dependent P-wave velocity intervals and the velocity profiles extracted from seismic tomography provides estimates of the depths of the main intra-crustal interfaces.

The comparison between tomographic velocities and borehole data (Fig. 7) shows a general agreement in the shallow crust, where velocity-derived lithological boundaries are consistent with the stratigraphic information available from the well. Differences between velocity-based classification and borehole observations may occur within the uncertainty range associated with both datasets, particularly for lithologies characterized by broad velocity distributions. These differences reflect the combined effects of velocity variability, resolution limits of the tomographic model, and the simplifying assumptions inherent in the petrophysical classification scheme.

The petrophysical approach was then extended to the full 3D model domain, assigning each cell to a lithological unit based on the corrected vp ranges. This procedure allowed the reconstruction of intra-crustal surfaces corresponding to major lithological transitions, including the top of carbonate platforms, the boundary with underlying siliciclastic units, and deeper transitions within the crystalline crust (Fig. 3c).

The final 3D crustal architecture results from the integration of the petrophysical classification with independent constraints from geological maps, borehole data, gravity models, and seismic profiles, ensuring consistency between the velocity-based classification and available geological and geophysical observations.

Building on the 1D application, the methodology was extended to the 3D tomographic volume to delineate the main crustal boundaries across the study area and reconstruct the surfaces representing key intra-crustal discontinuities.

https://doi.org/10.5194/essd-2026-513
Preprint. Discussion started: 9 September 2026

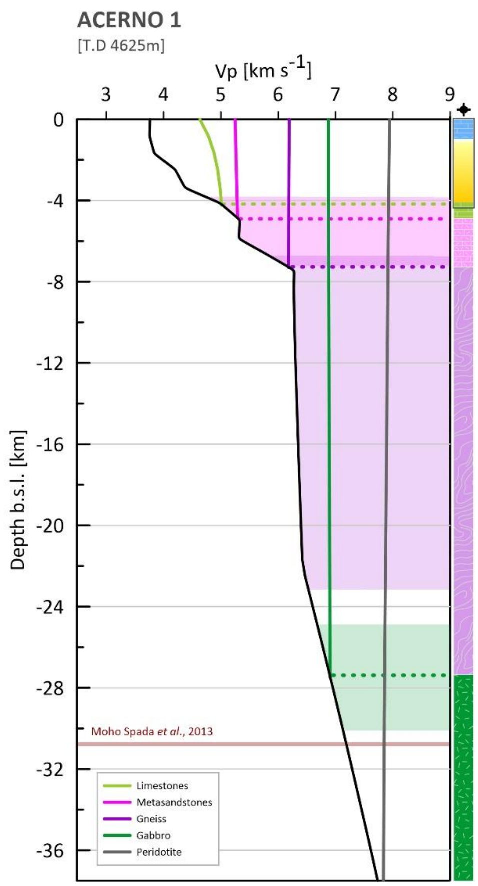

475 **Figure 7: Seismic velocity-depth profile and lithological interpretation at the Acerno 1 well location**. The black line shows the local P-wave velocity profile (v_p in km s^{-1}) from the tomographic model, plotted against depth b.s.l. Colored lines represent the $V_{p0}^{central}$ for key lithologies (Table 2): limestones (pale green), metasandstones (magenta), gneiss (purple), gabbro (green), and peridotite (grey). Specifically, limestone compaction trend is based on the *Wyllie equation*. Horizontal dashed lines mark interpreted transitions. The Moho from Spada et al. (2013) is shown as a solid red line. In the upper right corner, the interpreted
480 lithological log of the Acerno 1 well (Ferranti et al., 2024) is shown; it is used as a reference for constraining the shallow portion of the retrieved interface.

https://doi.org/10.5194/essd-2026-513
Preprint. Discussion started: 9 September 2026

5. 3D Crustal Model

The application of the depicted petrophysical approach enabled the construction of a three-dimensional, regional-scale crustal model of the Southern Apennines. Fig. 8 illustrates the retrieved intra-crustal discontinuities that define the interfaces between the representative lithological units identified within the lithostratigraphic framework (Fig. 3c).

Panel (a) of Fig. 8 shows the topographic surface derived from the TINITALY 1.1 dataset (Tarquini et al., 2023), together with the study area and the main regional tectonic lineaments, including the outcropping thrust fronts numbered from [1] to [3] (Fig. 3a,b). In the same panel (a), it is also shown the location of the outcropping Campanian sedimentary basins and the Apulian carbonate platform.

Panels (b-f) of Fig. 8 display depth maps of the main intra-crustal discontinuities. Panel (b) shows the top of the Mesozoic carbonate platform; panel (c) the top of the metasandstones underlying the carbonate sequence; panel (d) the top of the Hercynian gneissic crystalline basement; panel (e) the gabbroic transition marking the boundary between upper and lower crustal domains; and panel (f) the Moho discontinuity derived from Spada et al. (2013). The major tectonic lineaments are projected down to the top of the metasandstones, while their deeper geometry is not resolved within the scope of this model. The Sangineto Fault is assumed to intersect the gabbroic transition surface, in agreement with its mapped regional position (Ghisetti and Vezzani, 1981).

In the initial stage of the modeling, a single surface was defined to represent the top of the Mesozoic carbonate sequence (Fig. 8b), without distinction between Apenninic and Apulian domains. This surface was derived from the petrophysical workflow (Fig. 7), using vp values around 5.0 ± 0.4 km/s, consistent with previous studies (Barchi et al., 1998; Finetti, 2001-2005). The incorporation of structural information, including the geometry of major thrust ramps (Vezzani et al., 2010), allowed subdivision of this surface into distinct sectors corresponding to the Apenninic and Apulian carbonate platforms. This subdivision is not associated with clear lateral vp contrasts, but results from the integration of structural and geological constraints. The geometry of the carbonate surface (Fig. 8b) shows a progressive deepening from the internal domains toward the axial zone of the chain. In the western sector, the carbonate units occur at shallow depths, locally approaching surface exposure, whereas toward the central Apennines the surface reaches depths of approximately 10 km b.s.l. East of structure [3], the Apulian platform is exposed and deepens westward beneath the orogenic belt.

The top of the crystalline basement is constrained through the identification of velocity contrasts associated with metasandstones and gneissic units (Table 2; Fig. 6). Panels (c) and (d) of Fig. 8 show the depth of the metasandstone layer and the underlying gneissic basement, respectively, ranging from approximately −4 to −10 km b.s.l. and -6 to -13 km b.s.l.

A comparison between these two surfaces highlights a limited vertical separation and, locally, a convergence of the two interfaces. This behavior reflects the partial overlap in velocity ranges assigned to metasandstones and gneissic lithologies (Fig. 6), which introduces uncertainty in the identification of a sharp boundary between these units. This effect is particularly evident in areas of lower model resolution or limited data constraints.

The gabbroic transition surface (Fig. 8e) shows a regional-scale geometry characterized by a broad depression aligned with the Apennine chain. Additional local variations are observed in the central and southern sectors of the model domain. The vertical distance between the gabbroic surface and the Moho varies laterally, ranging from approximately 5-7 km in the Tyrrhenian sector to 10-13 km in the Adriatic domain (Fig. 8f).

The Moho discontinuity (Fig. 8f), derived from Spada et al. (2013), defines the lower boundary of the model and constrains the total crustal thickness across the study area. Additional information and datasets related to the unified Moho surface adopted throughout the study area are provided in *Supplementary Note 3* of the Supplementary Material (Table 3).

The 3D rendering of the crustal domains and two representative cross-sections are shown in Fig. 9. The model integrates intra-crustal surfaces, the major tectonic features, and the available constraints on the geometry of upper-crustal structures, resulting in a consistent 3D representation of the regional-scale crustal architecture.

Panel (a) of Fig. 9 illustrates the volumetric model, including the spatial distribution of lithostratigraphic units and major tectonic features. Thrust planes are extrapolated to depth using dip angles derived from literature data (Vezzani et al., 2010; Scandone et al., 2004; Patacca et al., 2008). Panels (b) and (c) show two cross-sections extracted from the model: a Campi Flegrei-Gargano transect and a section corresponding to the CROP 04 profile. These sections highlight the lateral variability of crustal units and the geometry of intra-crustal discontinuities across the model domain.

The complete set of intra-crustal surfaces displayed in Fig.8 is available in *Supplementary Note 4* of the Supplementary Material (Table 3).

https://doi.org/10.5194/essd-2026-513
Preprint. Discussion started: 9 September 2026

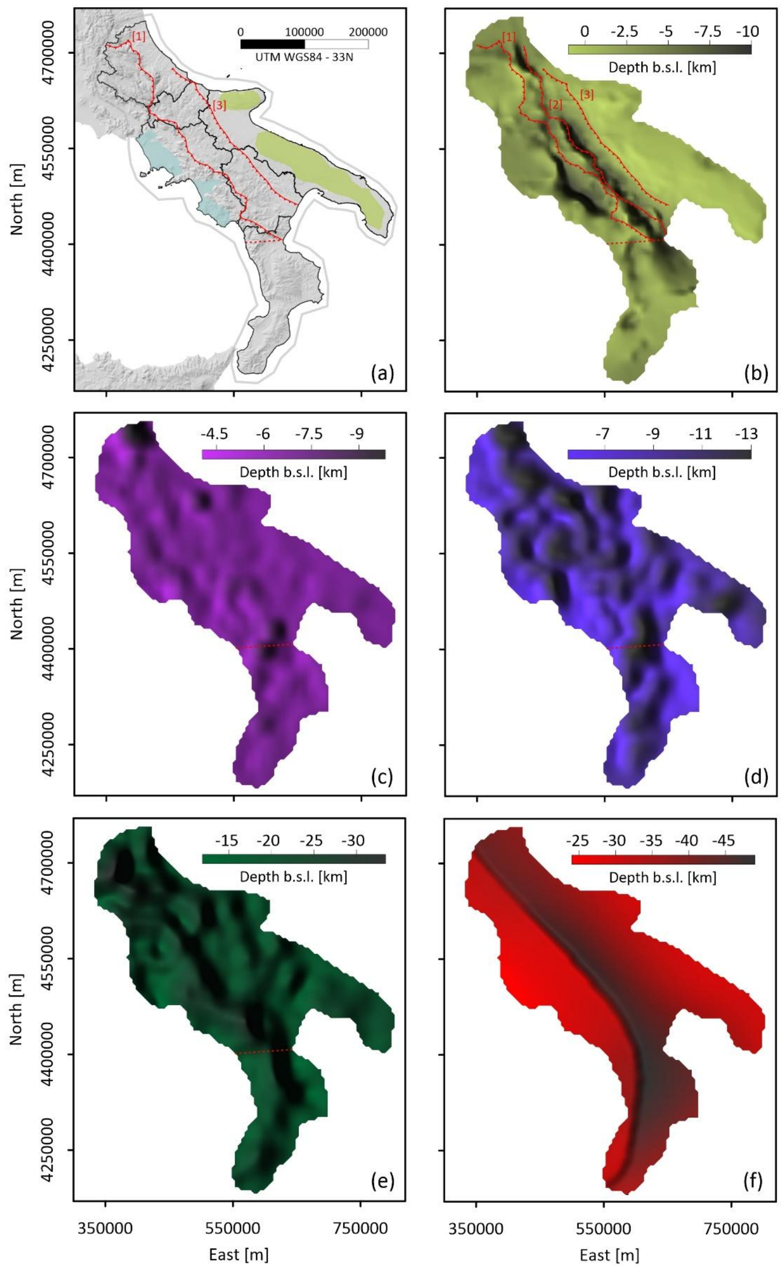

Figure 8: **Retrieved main intra-crustal discontinuities of the Southern Apennines.** (a) SRTM DEM of the study area on which the main regional tectonic lineaments (red lines) and the traces of the major thrust features (numbers [1]-[3]) are shown. Outcropping areas of the Apulian carbonate platform (green) and Campanian sedimentary basins (light blue) are shown. The grey-shaded polygon outlines the buffer zone of the investigated area. (b) Depth to the top of the carbonate platform. (c) Depth to the top of the metasandstones. (d) Depth to the top of the gneissic crystalline basement. (e) Depth to the gabbroic transition within the mafic lower crust. (f) Depth to the Moho discontinuity from Spada et al. (2013).

https://doi.org/10.5194/essd-2026-513
Preprint. Discussion started: 9 September 2026

Open Access Earth System Science Data Discussions

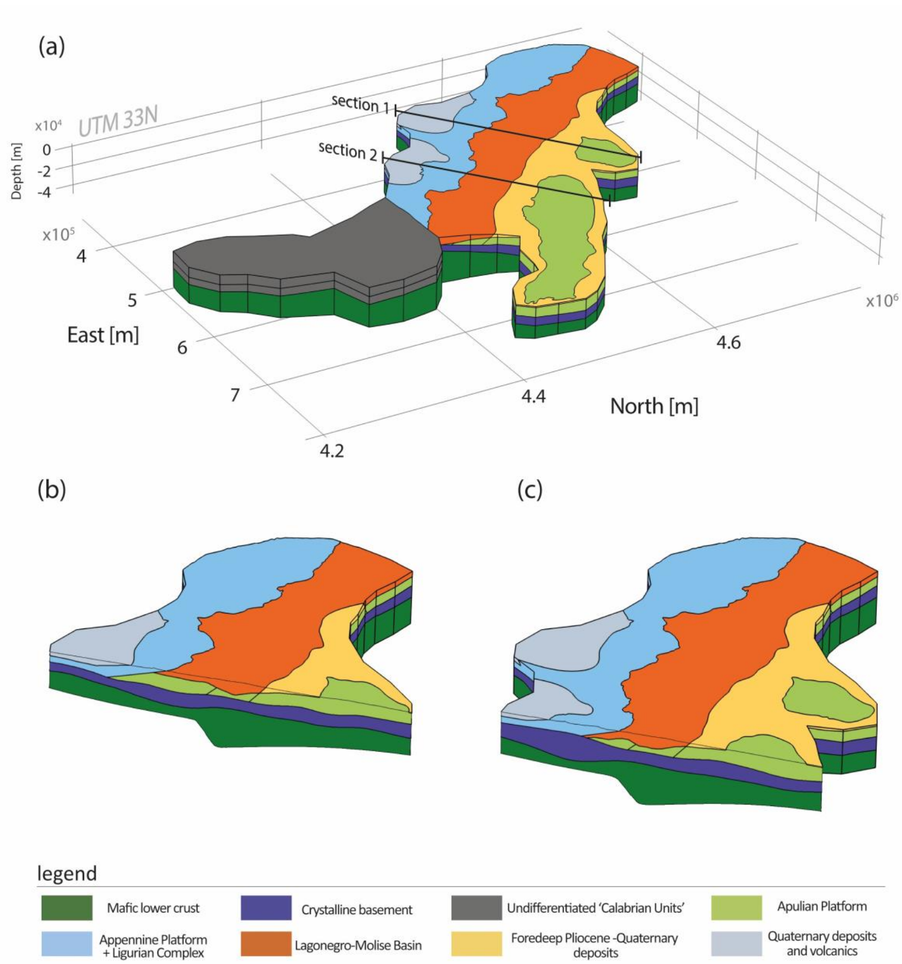

Figure 9: **3D integrated crustal model.** (a) Overview of the finalized 3D crustal model showing the traces of two reference cross-sections. (b) Section 1 - Campi Flegrei-Gargano transect; (c) Section 2 - CROP 04 profile. All coordinates are expressed in the UTM WGS84 coordinate system, zone 33N.

6. Model Validation

The spatial distribution and coverage of the independent datasets used for model validation are shown in Fig. 10. Validation was performed by integrating direct geological constraints with independent geophysical information, adopting different strategies for the upper and lower crust according to the availability of reference data. Different strategies were adopted for the analysis of upper and lower crust, reflecting the variable availability of reference data. In the upper crust, the top of the carbonate platforms was validated using direct borehole information and potential field- derived surfaces (Fig. 11). Deeper discontinuities, including the crystalline basement and Moho, were assessed against regional seismic profiles and interpreted gravity and magnetic models (Fig. 12). This multi-source validation approach ensured internal consistency and geophysical plausibility across the proposed 3D model. The datasets and reference surfaces used for model validation are fully documented and provided in Table 3 and *Supplementary Note 6* of the Supplementary Material.

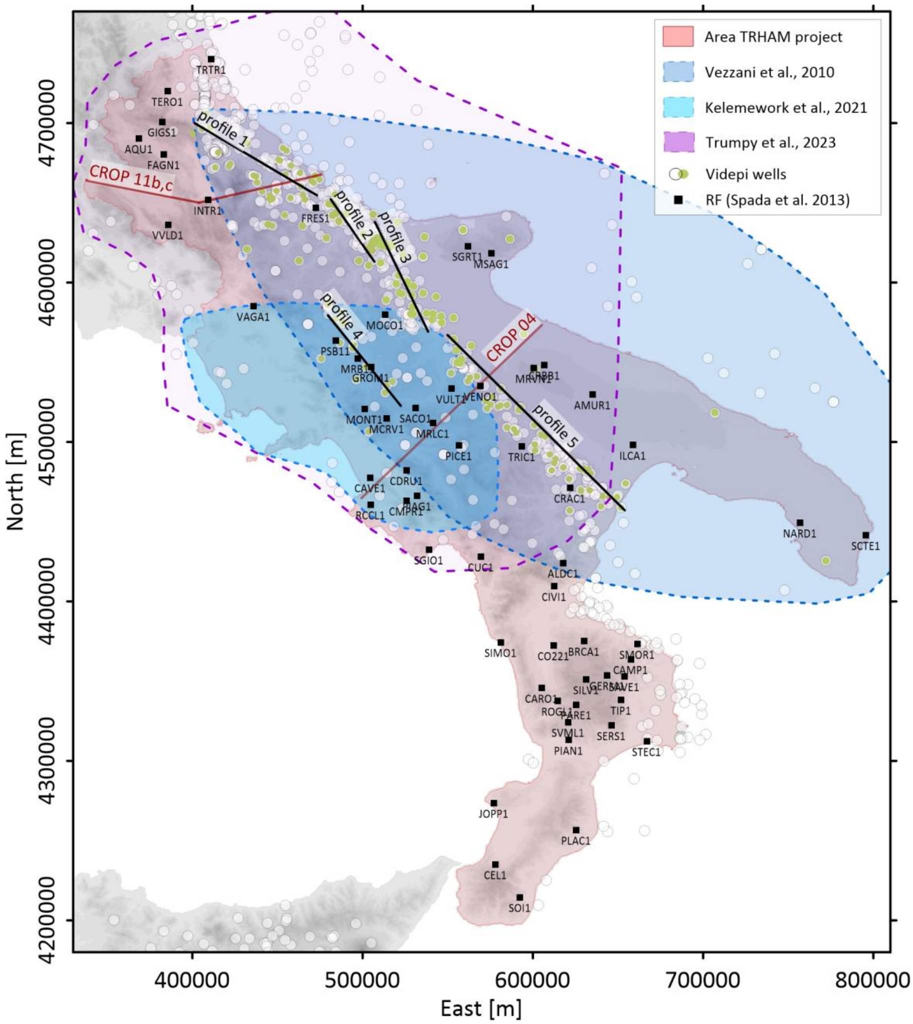

Figure 10: **Map of data coverage used for validation.** Colored polygons indicate the spatial extent of regional models for the top of key stratigraphic units: the Apulian and Campanian Mesozoic carbonate sequences from Vezzani et al. (2010; blue) and Kelemework et al. (2021a; light blue), respectively, and the Hercynian basement from Trumpy et al. (2023; violet). White circles mark all boreholes from the ViDEPI database, while green circles highlight those intersecting the top of the Mesozoic carbonate units. Black squares denote receiver function (RF) stations from Spada et al. (2013). Black lines represent the validation sections (from 1 to 5), passing through the largest number of videpi wells that intersect the carbonate platform, while in red regional geophysical cross-sections (CROP 04 and 11) for deeper model portion.

Top of Mesozoic Carbonates

In the upper portion of the model, particular attention was dedicated to accurately delineating the top of the Mesozoic carbonate platforms, representing a key regional marker. This surface is well constrained in parts of the study area by regional-scale interpretations, such as those by Vezzani et al. (2010) and Kelemework et al. (2021a), derived from geological cross-sections and potential field data. However, these sources do not provide full spatial coverage across the study area (see map in Fig. 10). Consistency was evaluated across all sources by cross-

https://doi.org/10.5194/essd-2026-513
Preprint. Discussion started: 9 September 2026

checking the resulting surface with the Vezzani et al. (2010) and Kelemework et al. (2021a) datasets, as well as with lithostratigraphic constraints from deep wells in the ViDEPI database that intersect the Mesozoic carbonate succession within the study area.

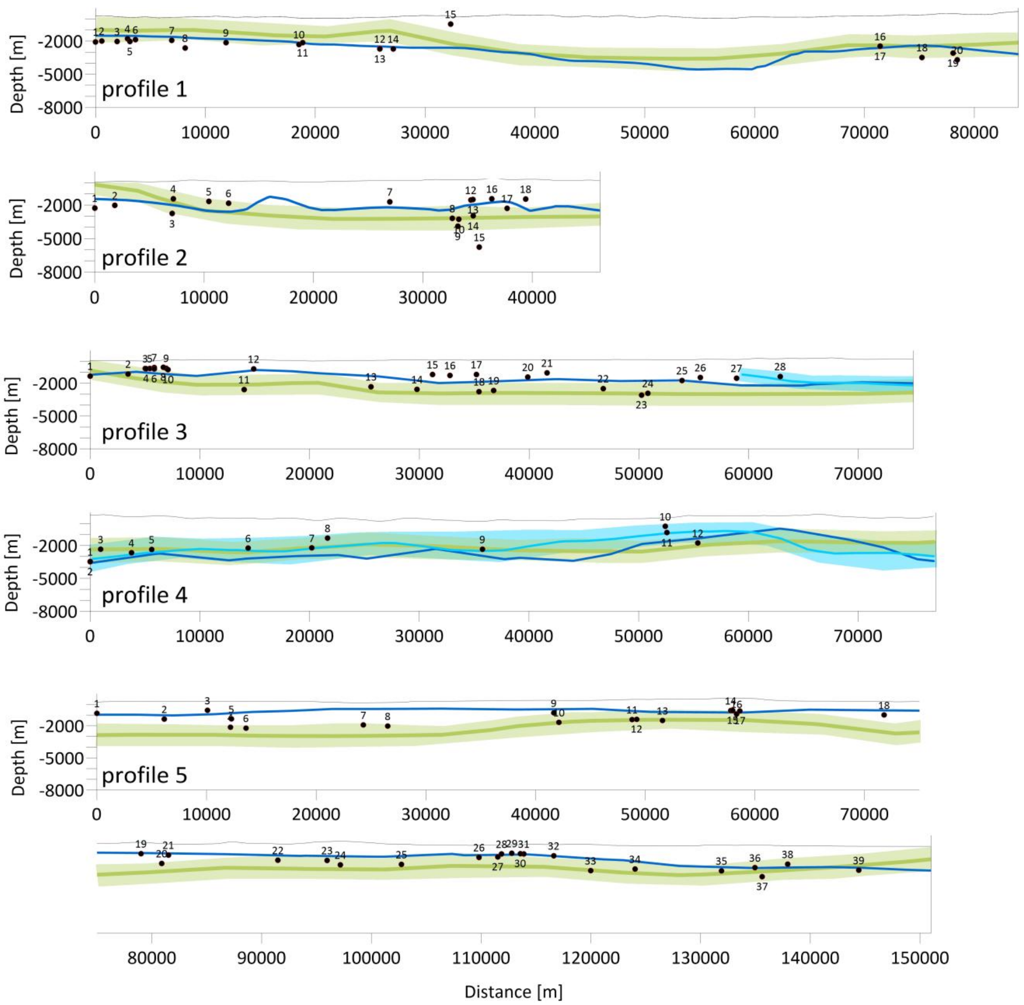

Figure 11: **Validation of the depth to the top Mesozoic carbonate platform.** The thin black line depicts the surface topography along each cross-section shown in Fig. 9. The green line marks the depth corresponding to the 5.0 km/s v_p isosurface, and the surrounding green shaded envelope represents the ±0.2 km/s uncertainty range. The blue line shows the top of the carbonate units as interpreted by Vezzani et al. (2010), whereas the sky-blue line illustrates the carbonate boundary derived from Kelemework et al. (2021a), with its associated error range indicated by the shaded band. Black dots indicate the depth of the top of the Mesozoic limestones from the ViDEPI wellbore dataset (the names and location of all wells are provided in *Supplementay Note 6* in Supplementary Materials).

Top crystalline basement and felsic-to-mafic crustal transition

Due to the absence of direct geological constraints at these depths, the validation of our model relies on independent geophysical interpretations. In particular, we compare our results with regional-scale seismic

https://doi.org/10.5194/essd-2026-513
Preprint. Discussion started: 9 September 2026

reflection profiles and with the gravity and magnetic interpretations presented in Kelemework et al. (2021a), which provide coherent information on the deep crustal architecture across the study area (Fig. 10). According to Kelemework et al. (2021a,b), the uncertainty in the estimated depth of key crustal boundaries varies along the profiles. The depth to the top of the crystalline basement is relatively well constrained (±0.1-1.5 km), with smaller uncertainties beneath the Tyrrhenian coast and the Apulian platform, and larger values beneath the Apennine thrust-and-fold belt. The depth to the bottom of the magnetic sources is more uncertain, ranging from about ±2 km near the Tyrrhenian sector to ±4 km beneath the Apennines. Similarly, the Moho depth inferred from gravity gradients shows uncertainties of about ±2 km in the Tyrrhenian domain, increasing to ±4.5 km in the Apennine belt. These trends reflect the general increase in uncertainty with depth. Additionally, the regional extent and depth of the crystalline basement are further constrained by the depth-converted seismic interpretation provided by Trumpy et al. (2023), which offers an important complementary reference for the present study.

The Fig. 12 compares the model-derived crustal boundaries with independent geophysical interpretations along the regional seismic transects CROP 04 and CROP 11b/c. As discussed previously, the top of the crystalline basement may correspond, at the crustal scale, to either metasandstones or gneissic units. To illustrate this, the figure is organized into two panels: (Fig. 12a) shows the configuration using metasandstones as the basement top, and (Fig. 12b) shows the configuration using gneiss. In both panels, the felsic-to-mafic crustal transition (green line) and the Moho (red line, from Spada et al., 2013) are displayed. The shaded envelopes surrounding each modeled boundary represent the v_p variability associated with each lithology (Table 2), indicating the expected depth uncertainty.

When the metasandstone surface is considered (panel a), the resulting top of the crystalline basement (pink line and shading) shows a reasonable correspondence with the basement depth from Trumpy et al. (2023), particularly in the eastern part of CROP 04 and the western part of CROP 11. In these areas, the mismatch is on the order of ~3 km along CROP 04 and ~4 km along CROP 11. However, this surface diverges more significantly from the gravity-derived basement of Kelemework et al. (2021a), with differences commonly reaching ~5 km along CROP 04 and ~7 km along CROP 11. In contrast, the gneiss-based configuration (panel b; violet line and shading) provides consistently better agreement with both the gravity-derived basement of Kelemework et al. (2021a) and the depth-converted basement from Trumpy et al. (2023), while also being associated with a narrower velocity-derived uncertainty range (Table 2; see also Fig. 6). For this reason, we consider it reliable to assume the gneiss surface as the most representative depth to the crystalline basement in our final crustal model.

Along both the CROP 04 and CROP 11b/c transects, the agreement between the modeled felsic-to-mafic transition (dark green line in panels a and b of Fig. 12) and independent geophysical constraints is strongest in the western sector, whereas larger discrepancies emerge toward the Apulian platform. In the western portions of the profiles, the modeled gabbroic unit lies very close to the Moho and falls within the ±4 km depth uncertainty associated with the Moho estimates of Kelemework et al. (2021a). This close correspondence is likely linked to crustal thinning and magmatic underplating associated with localized crustal delamination beneath the Tyrrhenian domain. By contrast, in the Apulian sector, the greater vertical separation between the gabbro and the Moho reflects a more continuous and well-preserved lower crustal succession, lacking significant crustal removal or mafic addition.

Overall, these comparisons indicate that the model effectively reproduces the large-scale crustal architecture across the region, including the geometry of the crystalline basement and the felsic-to-mafic crustal transition.

https://doi.org/10.5194/essd-2026-513
Preprint. Discussion started: 9 September 2026

Open Access Earth System Science Data Discussions

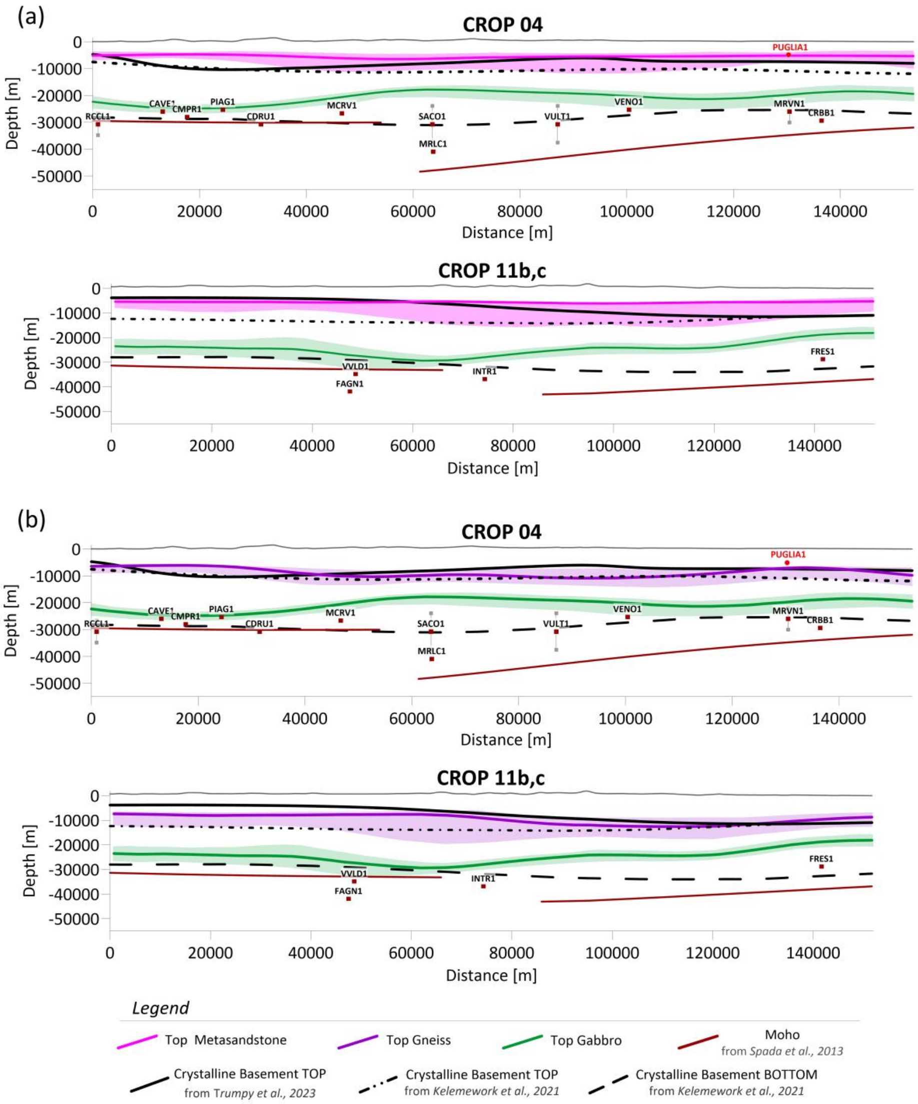

Figure 12: **Validation of deep crustal boundaries.** Regional geophysical cross-sections are shown in the overview map (Fig. 10). Panels (a) and (b) compare model-derived discontinuities with independent geophysical interpretations along the CROP 11b/c and CROP 04 seismic transects, respectively. The violet line represents the top of the gneissic transition, with the shaded violet envelope indicating the full range of v_p values assigned to this unit (Table 2). The magenta line marks the metasandstones, and the shaded magenta envelope indicates the corresponding v_p range. The green line denotes the top of the gabbroic crust (transition to mafic lower crust), with the shaded green envelope showing the complete v_p interval used for this lithology (Table 2). The red line marks the Moho discontinuity, directly adopted from Spada et al. (2013). Receiver function estimates along each transect are shown as red squares (mean depth) with grey squares indicating associated uncertainty. Surface topography is also shown (thin black line).

https://doi.org/10.5194/essd-2026-513
Preprint. Discussion started: 9 September 2026

7. Discussion

The integrated 3D crustal model presented in this study provides a coherent representation of the large-scale architecture of the Southern Apennines by combining seismic tomography (Magnoni et al., 2022), geological constraints (Vezzani et al., 2010), borehole information from the ViDEPI database (Ferranti et al., 2024), receiver-function estimates of Moho depth (Spada et al., 2013), and laboratory-derived petrophysical data compiled from the literature (e.g., Fountain, 1976; Christensen, N. I. and Mooney, 1995; Kern et al., 1996; Kono et al., 2009; Wang et al., 2013). The comparison with independent datasets demonstrates that the main lithological interfaces identified through the petrophysical approach are broadly consistent with existing geological and geophysical models (Kelemework et al., 2021a; Trumpy et al., 2023), despite the different resolution, assumptions, and data types involved.

A key outcome of the proposed methodology is the identification of regionally continuous crustal boundaries directly from a calibrated seismic velocity model. In particular, the comparison with independent geological and geophysical constraints indicates that the gneissic interface provides the most consistent representation of the crystalline basement at regional scale and is therefore adopted as the reference basement surface in the released model. The model also identifies a laterally continuous felsic-to-mafic crustal transition represented by the gabbroic interface, providing an additional crustal boundary that may be useful for future geological and geophysical investigations. The vertical relationship between this interface and the Moho discontinuity varies across the study area and constitutes one of the main structural features documented by the released dataset.

The proposed workflow is inherently affected by the limitations of the input datasets. The spatial resolution of the final model is primarily controlled by the resolution of the tomographic model (Magnoni et al., 2022), which varies with depth and seismic ray coverage. Furthermore, the lithological classification relies on representative laboratory velocity ranges corrected for pressure and temperature conditions (Fountain, 1976; Kern and Richter, 1981; Kern and Schenk, 1985), and therefore cannot fully account for local compositional heterogeneity, anisotropy, fluid content, or unresolved thermal variations. Consequently, the retrieved surfaces should be interpreted as regional-scale boundaries rather than sharp geological contacts.

Beyond the specific case of the Southern Apennines, the methodology provides a reproducible framework for integrating seismic tomography with petrophysical constraints under crustal pressure-temperature conditions. Because the approach relies on datasets that are commonly available in many tectonically active regions, it can be readily adapted to different geological settings and spatial scales. The released dataset may support a broad range of applications, including earthquake location, seismic imaging, gravity modelling, thermo-mechanical simulations, and crustal-scale geodynamic investigations (e.g., Magistrale et al., 1999; Molinari et al., 2011; Livani et al., 2022).

8. Data Availability

All datasets used and generated in this study have been deposited in a dedicated Zenodo repository (Perrini et al., 2026; https://doi.org/10.5281/zenodo.21130189). The repository is organized into thematic folders, each corresponding to one of the principal data categories used in this study. These folders contain the original datasets, intermediate processing products, derived model outputs, metadata, and auxiliary files associated with specific elements of the integrated 3D crustal model. Table 3 provides an overview of the repository structure, linking each thematic folder to the corresponding figures and tables in the manuscript and to its dedicated Supplementary Note (SN1-SN6). Each Supplementary Note serves as a user guide for its corresponding folder, documenting the data

https://doi.org/10.5194/essd-2026-513
Preprint. Discussion started: 9 September 2026

provenance, scientific rationale, processing workflow, file organization, formats, metadata, and the contents of every distributed file. Collectively, the Supplementary Notes facilitate repository navigation and enable users to efficiently identify, understand, reproduce, and reuse the datasets distributed with this study.

Table 3: Summary of the datasets available in the Zenodo repository associated with this study. The table lists the archived materials according to their scientific purpose and corresponding *Supplementary Notes* (SN1-SN6), and provides links to the figures and tables in which the datasets are used. Detailed file-level documentation is provided in the corresponding Supplementary Note available in the Supplementary Material.

Item	Reference Figure/Table	Description	Format(s)	Supplementary Note and Folder
Seismic tomography datasets	Figure 4, Table S1	Original, processed, and derived seismic tomography datasets used. Includes the original tomography of Magnoni et al. (2022), the resampled 3D velocity model (5 km × 5 km × 1 km resolution), metadata describing model geometry and discretization, and graphical documentation of the resampling procedure and spatial coverage.	.csv, .mat, .txt	SN1, SF1
Main regional structural features	Figure 3, Table S2	Digitized structural traces correspond to the 3 major regional tectonic features shown in Fig. 3. Files contain Easting and Northing coordinates in UTM Zone 33N and are provided for direct visualization and integration into GIS and geological modelling software.	.dat	SN2, SF2
Constraints on Moho *p-wave* velocities	Figures 8f, Table S3	Original, harmonized and derived datasets used to constrain Moho geometry and Moho P-wave velocities. Includes the original Adriatic and Tyrrhenian Receiver Function Moho surfaces from Spada et al. (2013), the complete RF station dataset, the harmonized Moho surface adopted in the TRHAM framework, the crystalline basement-bottom surface from Kelemework et al. (2021a), and the spreadsheet containing the station-by-station comparison between RF-derived discontinuity depths and seismic velocities extracted from the tomography of Magnoni et al. (2022).	.grd, .dat, .txt, .xlsx	SN3, SF3
Modelled intra-crustal transition surfaces	Figure 8, Table S4	Geological and geophysical surfaces used to construct the integrated 3D crustal model in Figure 8. The provided repository includes the original DEM from Tarquini et al. (2023), the harmonized Moho surface adopted in this study, and derived surfaces representing the tops of the main lithological units (sandstones, limestones, gneiss, and gabbro). Surfaces are provided in both grid and ASCII formats to facilitate reuse.	.dem, .grd, .dat	SN4, SF4
Pressure-temperature corrected p-wave velocities	Figure 6, Table S5	Original and derived datasets used to generate pressure- and temperature-corrected velocity models. Includes lithology-dependent correction datasets, reference velocity–depth profiles, supplementary corrected profiles presented in Figure S2, and all files required to reproduce the petrophysical workflow.	.txt, .xlsx	SN5, SF5
Reference surfaces and borehole constraints used for model validation	Figures 10-12, Table S6	Independent datasets used for model validation. Includes geological surfaces digitized from Vezzani et al. (2010) and Trumpy et al. (2023), reference magnetic crystalline basement top and bottom surfaces from Kelemework et al. (2021a), borehole compilations extracted from the VIDEPI database, and profile-specific borehole datasets used in the validation analyses and geological cross-sections.	.grd, .dat, .txt, .xlsx	SN6, SF6

https://doi.org/10.5194/essd-2026-513
Preprint. Discussion started: 9 September 2026

Open Access Earth System Science Data Discussions

9. Conclusion

This study presents a new 3D crustal model of the Southern Apennines together with the associated digital dataset and methodological workflow. The model was constructed by integrating seismic tomography, laboratory-derived petrophysical constraints, geological information, borehole observations, and independent geophysical datasets. The released dataset includes the main reconstructed intra-crustal discontinuities and the corresponding integrated 3D crustal model. Validation against independent geological and geophysical constraints indicates an overall consistency of the reconstructed surfaces within the uncertainty limits of the input datasets.

Beyond the Southern Apennines, the proposed workflow provides a reproducible framework for integrating seismic tomography and petrophysical information in regions characterized by complex crustal architecture. The dataset may support future geological, geophysical, and seismological applications and can serve as a reference model for further investigations of the crustal structure of the Southern Apennines.

This study was conducted within the framework of the TRHAM project (Relation between 3D Thermo-Rheological model and seismic HAzard for risk Mitigation in the urban areas of Southern Italy), funded by the Italian PRIN 2022 PNRR programme. The integrated three-dimensional crustal model presented here constitutes the geological and geophysical basis for subsequent thermo-rheological and seismic hazard investigations in Southern Italy.

https://doi.org/10.5194/essd-2026-513
Preprint. Discussion started: 9 September 2026

Author contributions

Conceptualization: R.C., G.D.L.
Methodology: M.P., R.C., G.G., V.K.
Data Curation: M.P., G.G., V.K.
Formal Analysis / Investigation: M.P., F.A., A.Z.
Validation: M.P., V.K., D.D.N., M.M.C.C., R.C., G.F., M.T.
Writing - Original Draft: M.P., G.D.L., R.C., G.G., V.K., M.F.
Writing - Review & Editing: All authors
Supervision: G.D.L., R.C.
Funding Acquisition: R.C., G.D.L., M.M.C.C.

Competing interests

The authors declare no competing interests.

Disclaimer

Copernicus Publications remain neutral with regard to jurisdictional claims made in the text, published maps, institutional affiliations, or any other geographical representation in this paper. While Copernicus Publications makes every effort to include appropriate place names, the final responsibility lies with the authors. Views expressed in the text are those of the authors and do not necessarily reflect the views of the publisher.

Acknowledgements

This work was carried out within the framework of the TRHAM "*Relation between 3D thermo-rheological modelling and seismic hazard for risk mitigation in urban areas of southern Italy*" funded by the Next Generation EU, PRIN 2022 PNRR (code: P202299L2C).

Financial support

This research was funded by the TRHAM project *"Relation between 3D thermo-rheological modelling and seismic hazard for risk mitigation in urban areas of southern Italy"*, supported by the Next Generation EU programme, PRIN 2022 PNRR (code: P202299L2C).

https://doi.org/10.5194/essd-2026-513
Preprint. Discussion started: 9 September 2026

References

Aldinucci, M., Gandini, A., and Sandrelli, F.: The Mesozoic continental rifting in the Mediterranean area: Insights from the Verrucano tectofacies of southern Tuscany (Northern Apennines, Italy), *Int. J. Earth Sci.*, 97, 1247-1269, https://doi.org/10.1007/s00531-007-0208-9, 2008.

Amodio-Morelli, L., Bonardi, G., Colonna, V., Dietrich, D., Giunta, G., Ippolito, F., Liguori, V., Lorenzoni, S., Paglionico, A., Perrone, V., Piccarreta, G., Russo, M., Scandone, P., Zanettin-Lorenzoni, E., and Zuppetta, A.: L'arco calabro-peloritano nell'orogene Appenninico-Maghrebide, *Mem. Soc. Geol. Ital.*, 17, 1-60, 1976.

Amoroso, O., Ascione, A., Mazzoli, S., Virieux, J., and Zollo, A.: *Seismic imaging of a fluid storage in the actively extending Apennine mountain belt, southern Italy*, Geophys. Res. Lett., 41, 3802–3809, https://doi.org/10.1002/2014GL060070, 2014.

Barberini, V., Burlini, L., and Zappone, A.: Elastic properties, fabric and seismic anisotropy of amphibolites and their contribution to the lower crust reflectivity, *Tectonophysics*, 445, 227-244, https://doi.org/10.1016/j.tecto.2007.08.017, 2007.

Barchi, M., Minelli, G., and Pialli, G.: The CROP 03 profile: A synthesis of results on deep structures of the northern Apennines, *Mem. Soc. Geol. Ital.*, 52, 383-400, 1998.

Boccaletti, M., Calamita, F., Carbone, S., Centamore, E., Cherchi, A., and Ciaranfi, N.: Palinspastic restoration and paleogeographic reconstruction of the peri-Tyrrhenian area during the Neogene, *Palaeogeogr. Palaeoclimatol. Palaeoecol.*, 77, 41-50, 1990.

Bonardi, G., D'Argenio, B., and Perrone, V.: *Carta Geologica dell'Appennino Meridionale*, Mem. Soc. Geol. Ital., 41, scale 1:250 000, 1 sheet, 1988

Bosellini, A.: The western passive margin of Adria and its carbonate platforms, *Spec. Vol. Ital. Geol. Soc. 32nd Int. Geol. Congr.*, Florence, 79-92, 2004.

Brocher, T. M.: Empirical relations between elastic wave speeds and density in the Earth's crust, *U.S. Geol. Surv. Open-File Rep.*, 2005-1317, 2005.

Brozzetti, F.: *The Campania–Lucania Extensional Fault System, southern Italy: A suggestion for a uniform model of active extension in the Italian Apennines*, Tectonics, 30, TC5009, https://doi.org/10.1029/2010TC002794, 2011

Brückl, E., Behm, M., Decker, K., Grad, M., Guterch, A., Keller, G. R., and Thybo, H.: *Crustal structure and active tectonics in the Eastern Alps*, Tectonics, 29, TC2011, https://doi.org/10.1029/2009TC002491, 2010

Butler, R. W. H., Mazzoli, S., Corrado, S., De Donatis, M., Di Bucci, D., Gambini, R., Naso, G., Nicolai, C., Scrocca, D., Shiner, P., and Zucconi, V.: *Applying thick-skinned tectonic models to the Apennine thrust belt of Italy: Limitations and implications*, in: Thrust Tectonics and Hydrocarbon Systems, edited by: McClay, K. R., AAPG Memoir, 82, 647–667, 2004.

Camanni, G., De Landro, G., Mazzoli, S., Michele, M., Muzellec, T., Ascione, A., Schaff, D.P., Tarantino, S. and Zollo, A., 2025. Remobilization of inverted normal faults drives active extension in the axial zone of the southern Apennine mountain belt (Italy). *J. of the Geo. Soc.*, 182(2), pp.jgs2024-184.

Capdeville, Y. and Marigo, J.: Shallow layer correction for spectral element like methods, *Geophys. J. Int.*, 172, 1135-1150, https://doi.org/10.1111/j.1365-246X.2007.03642.x, 2008.

Carbone, S., Catalano, S., Lentini, F., and Monaco, C.: Le unità stratigrafico-strutturali dell'Alta Val d'Agri (Appennino Lucano) nel quadro dell'evoluzione del sistema catena-avanfossa, *Mem. Soc. Geol. Ital.*, 41, 331-341, 1988.

Carmignani, L., Decandia, F. A., Disperati, L., Fantozzi, P. L., Kligfield, R., Lazzarotto, A., et al.: Inner Northern Apennines, in *Anatomy of an Orogen: The Apennines and Adjacent Mediterranean Basins* (eds Vai, G. B. and Martini, I. P.), 197-213, Springer, https://doi.org/10.1007/978-94-015-9829-3_12, 2001.

Casero, P., Roure, F., Endignoux, L., Moretti, I., Muller, C., Sage, L., and Vially, R.: Neogene geodynamic evolution of the southern Apennines, *Mem. Soc. Geol. Ital.*, 41, 109-120, 1988.

Catalano, S., Monaco, C., and Tortorici, L.: Neogene-Quaternary tectonic evolution of the Southern Apennines, *Tectonics*, 23, TC2003, https://doi.org10.1029/2003TC001512, 2004.

https://doi.org/10.5194/essd-2026-513
Preprint. Discussion started: 9 September 2026

Cassinis, G., Durand, M., and Ronchi, A.: Remarks on the Permian and Permian-Triassic boundary in central and eastern Lombardy (Southern Alps, Italy), *J. Iber. Geol.*, 33, 133-142, 2007.

Cassinis, G., Perotti, C. R., and Ronchi, A.: Permian continental basins in the Southern Alps (Italy) and peri-Mediterranean correlations, *Int. J. Earth Sci.*, 101, 129-157, https://doi.org/10.1007/s00531-011-0642-6, 2012.

Cello, G. and Mazzoli, S.: Apennine tectonics in southern Italy: A review, *J. Geodyn.*, 27, 191-211, https://doi.org/10.1016/S0264-3707(97)00072-0, 1998.

Christensen, N. I. and Mooney, W. D.: Seismic velocity structure and composition of the continental crust: A global view, *J. Geophys. Res. Solid Earth*, 100, 9761-9788, https://doi.org/10.1029/95JB00259, 1995.

Cosentino, D., Cipollari, P., and Marsili, P.: Geology of the Central Apennines: A regional review, *Boll. Soc. Geol. Ital.*, 122, 7-56, 2003.

Cotecchia, V.: Le acque sotterranee e l'intrusione marina in Puglia: dalla ricerca all'emergenza nella salvaguardia della risorsa, *Mem. Descr. Carta Geol. Ital.*, XCII, 31-510, 2014.

D'Andrea, S., Pasi, R., Bertozzi, G., and Dattilo, P.: *Geological model, advanced methods help unlock oil in Italy's Apennines*, Oil Gas J., 91, 53–57, 1993.

Della Vedova, B., Bellani, S., Pellis, G., and Squarci, P.: Deep temperatures and surface heat flow distribution, in *Anatomy of an Orogen: The Apennines and Adjacent Mediterranean Basins* (eds Vai, G. B. and Martini, I. P.), 65-76, Springer, 2001.

De Landro, G., Vanorio, T., Muzellec, T., Russo, G., Lomax, A., Virieux, J., & Zollo, A. (2025). 3D structure and dynamics of Campi Flegrei enhance multi-hazard assessment. *Nat. Comm.*, 16(1), 4814.

Di Stefano, R. and Ciaccio, M. G.: The lithosphere and asthenosphere system in Italy as inferred from the Vp and Vs 3D velocity model and Moho map, *J. Geodyn.*, 82, 16-25, 2014.

Di Stefano, R., Bianchi, I., Ciaccio, M. G., Carrara, G., and Kissling, E.: Three-dimensional Moho topography in Italy: New constraints from receiver functions and controlled source seismology, *Geochem. Geophys. Geosyst.*, 12, Q09006, https://doi.org/10.1029/2011GC003649, 2011.

Fedi, M.: Estimation of density, magnetization, and depth to source: A nonlinear and noniterative 3-D potential-field method, *Geophysics*, 62, 814-830, 1997.

Feriozzi, F., Improta, L., Maesano, F. E., De Gori, P., and Basili, R.: The 3D crustal structure in the epicentral region of the 1980, Mw 6.9, Southern Apennines earthquake: New constraints from the integration of seismic exploration data, deep wells, and local earthquake tomography, *Tectonics*, 43, e2023TC008056, 2024.

Ferranti, L., Iezzi, F., Bacchiani, A., Pavano, F., Bellini, D., Citterio, A., Calabrò, R., and Pasquà, C.: The role of inherited structural anisotropies during co-seismic surface faulting: The Pescopagano fault case study (Irpinia seismogenic area, Southern Italy), *J. Struct. Geol.*, 188, 105267, https://doi.org/10.1016/j.jsg.2024.105267, 2024.

Finetti, I. R. (ed.): CROP Project: Deep seismic exploration of the Central Mediterranean and Italy, Elsevier, ISBN 9780080457604, 2005.

Finetti, I. R., Boccaletti, M., Bonini, M., Del Ben, A., Geletti, R., Pipan, M., and Sani, F.: Crustal section based on CROP seismic data across the North Tyrrhenian-Northern Apennines-Adriatic Sea, *Tectonophysics*, 343, 135-163, https://doi.org/10.1016/S0040-1951(01)00141-X, 2001.

Fountain, D. M.: The Ivrea-Verbano and Strona-Ceneri zones, Northern Italy: A cross-section of the continental crust—New evidence from seismic velocities of rock samples, *Tectonophysics*, 33, 145-165, https://doi.org/10.1016/0040-1951(76)90054-8, 1976.

Ghisetti, F. and Vezzani, L.: Contribution of structural analysis to understanding the geodynamic evolution of the Calabrian Arc (Southern Italy), *J. Struct. Geol.*, 3, 371-381, 1981.

Ghisetti, F. and Vezzani, L.: Depth and modes of Pliocene-Pleistocene crustal extension of the Apennines (Italy), *Terra Nova*, 11, 67-72, https://doi.org/10.1046/j.1365-3121.1999.00227.x, 1999.

Goleby, B. R., Blewett, R. S., Fomin, T., Fishwick, S., Reading, A. M., Henson, P. A., Kennett, B. L. N., Champion, D. C., Jones, L., Drummond, B. J., and Nicoll, M.: An integrated multi-scale 3D seismic model of the Archaean Yilgarn Craton, Australia, *Tectonophysics*, 420, 75-90, 2006.

Granado, C., Muñoz-Martín, A., Olaiz, A. J., Fernández, O., and Druet, M.: 3D crustal-scale structure of the West Iberia margin: A novel approach to integrated structural characterization of passive margins, *Mar. Geophys. Res.*, 42, 10, 2021.

Improta, L., Iannaccone, G., Capuano, P., Zollo, A., and Scandone, P.: Inferences on upper crustal structure of the Southern Apennines (Italy) from seismic refraction investigations and subsurface data, *Tectonophysics*, 317, 275-298, 2000.

Livani, M., Petracchini, L., Benetatos, C., Marzano, F., Billi, A., Carminati, E., Doglioni, C., Petricca, P., Maffucci, R., Codegone, G., Rocca, V., Verga, F., and Antoncecchi, I.: *Subsurface geological and geophysical data from the Po Plain and the northern Adriatic Sea (north Italy)*, Earth Syst. Sci. Data, 15, 4261–4293, https://doi.org/10.5194/essd-15-4261-2023, 2023

Kern, H. and Richter, A.: Temperature derivatives of compressional and shear wave velocities in crustal and mantle rocks at 6 kbar confining pressure, *J. Geophys.*, 49, 47-56, 1981.

Kern, H. and Schenk, V.: Elastic wave velocities in rocks from a lower crustal section in southern Calabria (Italy), *Phys. Earth Planet. Inter.*, 40, 147-160, https://doi.org/10.1016/0031-9201(85)90126-8, 1985.

Kern, H., Gao, S., and Liu, Q. S.: Seismic properties and densities of middle and lower crustal rocks exposed along the North China Geoscience Transect, *Earth Planet. Sci. Lett.*, 139, 439-455, https://doi.org/10.1016/0012-821X(95)00240-D, 1996.

Khazanehdari, J., Rutter, E. H., and Brodie, K. H.: High-pressure-high-temperature seismic velocity structure of the midcrustal and lower crustal rocks of the Ivrea-Verbano zone and Serie dei Laghi, NW Italy, *J. Geophys. Res. Solid Earth*, 105, 13843-13858, https://doi.org/10.1029/2000JB900025, 2000.

Knott, S. D.: The Liguride complex of southern Italy: A Cretaceous to Paleogene accretionary wedge, *Tectonophysics*, 142, 217-226, 1987.

Kono, Y., Ishikawa, M., Harigane, Y., Michibayashi, K., and Arima, M.: P- and S-wave velocities of the lowermost crustal rocks from the Kohistan arc: Implications for seismic Moho discontinuity attributed to abundant garnet, *Tectonophysics*, 467, 44-54, https://doi.org/10.1016/j.tecto.2008.12.010, 2009.

Kelemework, Y., Milano, M., La Manna, M., et al.: Crustal structure in the Campanian region (Southern Apennines, Italy) from potential field modelling, *Sci. Rep.*, 11, 14510, https://doi.org/10.1038/s41598-021-93945-8, 2021a.

Kelemework, Y., Fedi, M., and Milano, M.: A review of spectral analysis of magnetic data for depth estimation, *Geophysics*, 86, J33-J58, https://doi.org/10.1190/geo2020-0268.1, 2021b.

Lombardi, D., Braunmiller, J., Kissling, E., and Giardini, D.: Moho depth and Poisson's ratio in the Western-Central Alps from receiver functions, *Geophys. J. Int.*, 173, 249-264, 2008.

Ludwig, W. J., Nafe, J. E., and Drake, C. L.: Seismic velocities in the Earth, in *The Sea*, Vol. 4 (ed. Maxwell, A.), 53-84, Wiley-Interscience, 1970.

Magistrale, H., McLaughlin, K., and Day, S.: *A geology-based 3D velocity model of the Los Angeles basin sediments*, Bull. Seismol. Soc. Am., 86, 1161–1166, 1996.

Magnoni, F., Casarotti, E., Komatitsch, D., Di Stefano, R., Ciaccio, M. G., Tape, C., Melini, D., Michelini, A., Piersanti, A., and Tromp, J.: Adjoint tomography of the Italian lithosphere, *Commun. Earth Environ.*, 3, 69, https://doi.org/10.1038/s43247-022-00397-7, 2022.

Masson, Y. and Virieux, J.: P-SV-wave propagation in heterogeneous media: Velocity-stress distributional finite-difference method, *Geophysics*, 88, T165-T183, 2023.

Mazzoli, S., Di Bucci, D., and Tozzi, M.: Structural development of the northern sector of the Southern Apennines, Italy, *Tectonics*, 19, 1015-1030, 2000.

Mazzoli, S., D'Errico, M., Aldega, L., Corrado, S., Invernizzi, C., Shiner, P., and Zattin, M.: *Tectonic burial and "young" (<10 Ma) exhumation in the southern Apennines fold-and-thrust belt (Italy)*, Geology, 36, 243–246, https://doi.org/10.1130/G24344A.1, 2008.

https://doi.org/10.5194/essd-2026-513
Preprint. Discussion started: 9 September 2026

Mazzoli, S., Ascione, A., Candela, S., Iannace, A., Megna, A., Santini, S., and Vitale, S.: *Subduction and continental collision events in the southern Apennines: constraints from two crustal cross-sections*, Rend. Online Soc. Geol. Ital., 25, 78–84, https://doi.org/10.3301/ROL.2013.07, 2013.

Menardi Noguera, A. and Rea, G.: Deep structure of the Campanian-Lucanian Arc (Southern Apennines, Italy): Thin-skinned or thick-skinned model for active thrusting?, *Tectonophysics*, 324, 195-218, 2000.

Molinari, I. and Morelli, A.: EPcrust: A reference crustal model for the European Plate, *Geophys. J. Int.*, 185, 352-364, https://doi.org/10.1111/j.1365-246X.2011.04940.x, 2011.

Monaco, C., Tortorici, L., and Paltrinieri, W.: Structural evolution of the Lucanian Apennines, southern Italy, *J. Struct. Geol.*, 20, 617-638, 1998.

Mostardini, F. and Merlini, S.: Appennino Centro Meridionale: Sezioni geologiche e proposta di modello strutturale, AGIP, 1986.

Muzellec, T., De Landro, G., Camanni, G., Adinolfi, G. M., and Zollo, A.: The complex 4D multi-segmented rupture of the 2014 Mw 6.2 Northern Nagano earthquake revealed by high-precision aftershock locations, *Tectonophysics*, 898, 230641, 2025.

Nicolai, C. and Gambini, R.: Structural architecture of the Southern Apennines and its role in the geodynamics of the Apennine belt, *Boll. Soc. Geol. Ital. Suppl.*, 7, 21-37, 2007.

Ogniben, L.: Relazione sul Modello Geodinamico Conservativo della Regione Italiana, ENEA, Rome, 1985.

Patacca, E. and Scandone, P.: Geology of Southern Apennines, *Boll. Soc. Geol. Ital. Suppl.*, 7, 75-119, 2007.

Patacca, E. and Scandone, P.: Late thrust propagation and sedimentary response in the thrust-belt-foredeep system of the Southern Apennines (Pliocene-Pleistocene), in *Anatomy of an Orogen: The Apennines and Adjacent Mediterranean Basins* (eds Vai, G. B. and Martini, I. P.), 301-318, Springer, https://doi.org/10.1007/978-94-015-9829-3_23, 2001.

Patacca, E., Scandone, P., Di Luzio, E., Cavinato, G. P., and Parotto, M.: Structural architecture of the central Apennines: Interpretation of the CROP-11 seismic profile from the Adriatic coast to the orographic divide, *Tectonics*, 27, TC3006, https://doi.org/10.1029/2005TC001917, 2008.

Piana Agostinetti, N. and Amato, A.: Moho depth and Vp/Vs ratio in peninsular Italy from teleseismic receiver functions, *J. Geophys. Res. Solid Earth*, 114, B06303, https://doi.org/10.1029/2008JB005899, 2009.

Prosser, G., Palladino, G., Avagliano, D., Coraggio, F., Bolla, E. M., Riva, M., and Catellani, D. E.: Stratigraphic and tectonic setting of the Liguride Units cropping out along the southeastern side of the Agri Valley (Southern Apennines, Italy), *Geosciences*, 11, 125, https://doi.org/10.3390/geosciences11030125, 2021.

Ricchetti, G., et al.: Geodinamica ed evoluzione sedimentaria e tettonica dell'avampaese apulo, *Mem. Soc. Geol. Ital.*, 41, 57-82, 1988.

Ricchetti, G. and Mongelli, F.: Flessione e campo gravimetrico della micropiastra Apula, *Boll. Geofis. Teor. Appl.*, 36, 381-398, 1980.

Rudnick, R. L. and Fountain, D. M.: Nature and composition of the continental crust: A lower-crustal perspective, *Rev. Geophys.*, 33, 267-309, 1995.

Savastano, L. and Piana Agostinetti, N.: Deep structure of the Southern Apennines as imaged by active and passive seismic data along the CROP-04 (crustal) reflection seismic profile, *J. Geol. Soc.*, 176, 1284-1290, https://doi.org/10.1144/jgs2018-201, 2019.

Scandone, P.: Studi di geologia lucana: nota illustrativa della carta dei terreni della serie calcareo-silico-marnosa, *Boll. Soc. Nat. Napoli*, 81, 1972.

Scandone, P., Mazzotti, A., Fradelizio, G. L., Patacca, E., Stucchi, E., Tozzi, M., and Zanzi, L.: Line CROP 04 - Southern Apennines, in *CROP Atlas: Seismic Reflection Profiles of the Italian Crust* (eds Scrocca, D., Doglioni, C., Innocenti, F., et al.), *Mem. Descr. Carta Geol. Ital.*, 62, 155-166, 2004.

Scrocca, D., Doglioni, C., and Innocenti, F.: Deep structure of the Southern Apennines (Italy): Thin-skinned or thick-skinned tectonics?, *Tectonics*, 22, 1058, https://doi.org/10.1029/2003TC001521, 2003.

Scrocca, D., Sciamanna, S., Di Luzio, E., Tozzi, M., Nicolai, C., and Gambini, R.: Structural setting along the CROP-04 deep seismic profile (Southern Apennines, Italy), *Boll. Soc. Geol. Ital. Suppl.*, 7, 283-296, 2007.

Shiner, P., Beccacini, A., and Mazzoli, S.: Thin-skinned versus thick-skinned structural models for Apulian carbonate reservoirs: Constraints from the Val d'Agri fields, *Mar. Pet. Geol.*, 21, 805-827, 2004.

Spada, M., Bianchi, I., Kissling, E., Piana Agostinetti, N., and Wiemer, S.: Combining controlled-source seismology and receiver-function information to derive a 3-D Moho topography for Italy, *Geophys. J. Int.*, 194, 1050-1068, https://doi.org/10.1093/gji/ggt148, 2013.

Spector, A. and Grant, F. S.: Statistical model for interpreting aero-magnetic data, *Geophysics*, 35, 293-302, https://doi.org/10.1190/1.1440092, 1970.

Tarquini, S., Isola, I., Favalli, M., Battistini, A., and Dotta, G.: *TINITALY, a digital elevation model of Italy with a 10 meters cell size (Version 1.1)* [data set], Istituto Nazionale di Geofisica e Vulcanologia (INGV), https://doi.org/10.13127/tinitaly/1.1, 2023.

Trumpy, E., Manzella, A., and Pertusati, P. C.: Regional scale surface of the top of the Variscan basement in the central sector of Italy, *J. Maps*, 19, https://doi.org/10.1080/17445647.2023.2243981, 2023.

Vitale, S., Ciarcia, S., Iannace, A., Mazzoli, S., D'Assisi Tramparulo, F., and Zaghloul, M. N.: *Evoluzione tettono-sedimentaria del Complesso d'Accrezione Liguride in Appennino Meridionale*, Rend. Online Soc. Geol. It., 25, 116–136, https://doi.org/10.3301/ROL.2013.11, 2013

Vezzani, L., Festa, A., and Ghisetti, F. C.: Geology and tectonic evolution of the Central-Southern Apennines, Italy, *Geol. Soc. Am. Spec. Pap.*, 469, https://doi.org/10.1130/2010.2469, 2010.

VIDEPI Project: Visibility of Petroleum Exploration Data in Italy, Italian Ministry of Economic Development, http://unmig.sviluppoeconomico.gov.it/videpi/en/pozzi/pozzi.asp, 2012.

Waldhauser, F.: A parametrized three-dimensional Alpine crustal model and its application to teleseismic wavefront scattering, PhD thesis, ETH Zürich, 1996.

Waldhauser, F., Kissling, E., Ansorge, J., and Mueller, S.: Three-dimensional interface modeling with two-dimensional seismic data: The Alpine crust-mantle boundary, *Geophys. J. Int.*, 135, 264-278, https://doi.org/10.1046/j.1365-246X.1998.00636.x, 1998.

Wang, Q., Bagdassarov, N., and Ji, S.: The Moho as a transition zone: A revisit from seismic and electrical properties of minerals and rocks, *Tectonophysics*, 609, 395-422, https://doi.org/10.1016/j.tecto.2013.08.041, 2013.

Wepfer, W. W. and Christensen, N. I.: A seismic velocity-confining pressure relation, with applications, *Int. J. Rock Mech. Min. Sci.*, 28, 451-456, https://doi.org/10.1016/0148-9062(91)90083-X, 1991.

Wyllie, M. R. J., Gregory, A. R., and Gardner, G. H. F.: Elastic wave velocities in heterogeneous and porous media, *Geophysics*, 21, 41-70, 1956.

Wyllie, M. R. J., Gregory, A. R., and Gardner, G. H. F.: An experimental investigation of factors affecting elastic-wave velocities in porous media, *Geophysics*, 23, 459-493, 1958.

Yegorova, T. P. and Starostenko, V. I.: Lithosphere structure of European sedimentary basins from regional three-dimensional gravity modeling, *Tectonophysics*, 346, 5-21, https://doi.org/10.1016/S0040-1951(01)00251-7, 2002.